# CANADIAN THESES

# THÈSES CANADIENNES

## NOTICE

The quality of this microfiche is heavily dependent upon the quality of the original thesis submitted for microfilming. Every effort has been made to ensure the highest quality of reproduction possible.

If pages are missing, contact the university which granted the degree.

Some pages may have indistinct print especially if the original pages were typed with a poor typewriter ribbon or if the university sent us an inferior photocopy.

Previously copyrighted materials (journal articles, published tests, etc.) are not filmed.

Reproduction in full or in part of this film is governed by the Canadian Copyright Act, R.S.C. 1970, c. C-30.

## AVIS

La qualité de cette microfiche dépend grandement de la qualité de la thèse soumise au microfilmage. Nous avons tout fait pour assurer une qualité supérieure de reproduction.

S'il manque des pages, veuillez communiquer avec l'université qui a conféré le grade.

La qualité d'impression de certaines pages peut laisser à désirer, surtout si les pages originales ont été dactylographiées à l'aide d'un ruban usé ou si l'université nous a fait parvenir une photocopie de qualité inférieure.

Les documents qui font déjà l'objet d'un droit d'auteur (articles de revue, examens publiés, etc.) ne sont pas microfilmés.

La reproduction, même partielle, de ce microfilm est soumise à la Loi canadienne sur le droit d'auteur, SRC 1970, c. C-30.

## THIS DISSERTATION HAS BEEN MICROFILMED EXACTLY AS RECEIVED

## LA THÈSE A ÉTÉ MICROFILMÉE TELLE QUE NOUS L'AVONS REÇUE

# Theoretical Study of $Yb^{3+}$ Spin-Lattice Relaxation Time and Monte Carlo Simulation of $Gd^{3+}$ EPR Linewidths in $Yb_xY_{1-x}Cl_3 \cdot 6H_2O$ Single Crystals

Ufuk Orhun

A Thesis

in

The Department

of

Physics

Presented in Partial Fulfillment of the Requirements
for the Degree of Master of Science at
Concordia University
Montréal, Québec, Canada

March 1986

ISBN 0-315-30689-0

## ABSTRACT

Theoretical Study of $Yb^{3+}$ Spin-Lattice Relaxation Time and Monte Carlo Simulation of $Gd^{3+}$ EPR Linewidths in $Yb_xY_{1-x}Cl_3 6H_2O$ Single Crystals

Ufuk Orhun

The objective of this thesis is to study $Yb^{3+}$ spin-lattice relaxation time in $Gd^{3+}$ doped $Yb_xY_{1-x}Cl_3 6H_2O$ single crystals, find its dependence on temperature so that the experimentally observed $Gd^{3+}$ EPR linewidths can be explained by spin-lattice relaxation narrowing mechanism, also to check by means of the Monte Carlo method if indeed the narrowing of $Gd^{3+}$ EPR linewidths is due to the spin-lattice relaxation process of $Yb^{3+}$ ions. An equation expressing $Yb^{3+}$ spin-lattice relaxation time as a function of temperature is derived which gives results in agreement with the relaxation narrowing and observed linewidths. The Monte Carlo simulation gave linewidths narrowing with decreasing $Yb^{3+}$ spin-lattice relaxation time. Therefore, it is concluded that the narrowing of $Gd^{3+}$ EPR lines is mainly due to the spin-lattice relaxation narrowing mechanism.

## ACKNOWLEDGEMENTS

The author is grateful to Professor S.K.Misra for proposing the studies covered in this thesis, and for his continued help and interest during the entire research. He also appreciates the teaching assistantship provided by the Department of Physics.

Lastly, but not the least, the author wishes to extend his appreciation to his family for their moral and financial assistance.

TABLE OF CONTENTS

# CHAPTER 1

## INTRODUCTION

EPR experiments on $Gd^{3+}$ doped $YbCl_3 6H_2O$ (to be referred to as YbCH hereafter) single crystals were done by Misra and Sharp[1] and by Malhotra et al.[2] In both cases temperature dependence of EPR linewidths of $Gd^{3+}$ ion were reported; it was suggested that this might have been due to the so called "random frequency modulation" effect. Misra and Mikolajczak[3] also reported temperature dependence of linewidths with $Gd^{3+}$ doped $Yb_xY_{1-x}Cl_3 6H_2O$ single crystals (to be referred to as $Yb_xY_{1-x}$CH hereafter).

Both $Gd^{3+}$ and $Yb^{3+}$ ions are paramagnetic, while $Y^{3+}$ ion is diamagnetic. In YbCH single crystals, $Gd^{3+}$ ion is almost completely surrounded by the host $Yb^{3+}$ ions (Gd/Yb ratio was 1/200); broadening of $Gd^{3+}$ EPR lines is expected to be due to the dipolar fields produced by the neighboring $Yb^{3+}$ ions. However as the temperature increases, so the $Yb^{3+}$ spin-lattice relaxation time $\tau_{Yb}$ decreases, there would be a random modulation of dipolar fields. This increased random modulation at higher temperatures reduces broadening effects and results in a narrowing of EPR lines with increasing temperature.

It is the purpose of this thesis, to simulate the random

relaxing $Yb^{3+}$ ions due to spin-lattice relaxation interactions by means of the Monte Carlo method in order to study the narrowing of the linewidth at higher temperatures. Prior to the simulation a theoretical study of $Yb^{3+}$ spin-lattice relaxation times in YbCH will be presented.

In the simulation, one thousand $Gd^{3+}$ ion sites, each with ten surrounding $Yb^{3+}$ neighbors were taken into account. Using the available crystal data the positions of $Yb^{3+}$ ions with respect to the $Gd^{3+}$ ion were found, enabling the calculation of $Yb^{3+}$ dipolar fields at a $Gd^{3+}$ site. With these dipolar fields, deviation of resonance frequency from Larmor frequency $\nu_L$ (due to the external magnetic field $H_z$) can be calculated. The neighboring ions relax at random times around a mean value, the rate of relaxation depending on temperature; thus, the frequency deviation changes with time as well as from one $Gd^{3+}$ site to another. Various spin-lattice relaxation time ratios:

$$\alpha = \tau_{Gd} / \tau_{Yb} \qquad (1)$$

will be used, corresponding to the changes in the temperature. Using Bloch's equations, absorption at each $Gd^{3+}$ site can be calculated. Finally a histogram can be plotted, using the modified EPR frequencies for one thousand $Gd^{3+}$ ion sites, for each value of $\alpha$. Similar calculations can be made for $Yb_xY_{1-x}CH$ where some of the $Yb^{3+}$ ions are

replaced by diamagnetic $Y^{3+}$ ions.

The results (Chapter 6) of the simulation yield a temperature dependence of the dipolar linewidth, to be compared with experimental observations. Also using the calculated $Yb^{3+}$ ion spin-lattice relaxation times and the results of the simulation, an estimation of $Gd^{3+}$ spin-lattice relaxation time and its dependence on temperature can be made.

# CHAPTER 2

## $Yb^{3+}$ SPIN-LATTICE RELAXATION TIME

The spin-lattice relaxation time $\tau_{Yb}$ of the $Yb^{3+}$ ion has been calculated using $Gd^{3+}$ EPR linewidths as a probe. However equations to calculate $\tau_{Yb}$ theoretically without using EPR linewidths of $Gd^{3+}$, given by Soeteman et al.[4] and Kalvius et al.[5] have not been in agreement with these.

### 2.1 CALCULATION OF $\tau_{Yb}$ FROM $Gd^{3+}$ LINEWIDTHS

Based on Anderson's[7] and Kubo-Tomita's[8] theory, $\tau_{Yb}$ (host ion) is given by

$$\tau_{Yb}=3h\Delta H_{1/2}/102(g\mu_B)^3 n^2 S(S+1)\mu_o^2 \qquad (2)$$

where $\Delta H_{1/2}$, h, g, $\mu_B$, n, S, and $\mu_o$ are respectively the guest $Gd^{3+}$ EPR linewidth, Planck's constant, g-value, Bohr magneton, number of host ions per unit volume, effective spin of host ion and permeability constant. Using this equation and the experimentally observed $Gd^{3+}$ linewidths by Misra and Sharp[1], $\tau_{Yb}$ values in YbCH are calculated. Also $\tau_{Yb}$ values are calculated in $Yb_xY_{1-x}CH$ using the experimentally observed $Gd^{3+}$ linewidths by Misra and Mikolajczak[3], for x=0.25, 0.50, 0.75. Log-log plots of $\tau_{Yb}$ as a function of temperature are shown in fig.1 for x=0.25,

0.50 and 0.75 and in fig.2 for x=1. For x=1 (YbCH), $\tau_{Yb}$ values calculated by Malhotra et al.[2], using the same equation, are also shown in fig.2. The differences between them are due to the variations in $\Delta H_{1/2}$ values observed experimentally.

No direct measurements of $Yb^{3+}$ spin-lattice relaxation times have been reported for temperatures above 40 K. Soeteman et al.[4] have measured $\tau_{Yb}$ by the dispersion-absorption technique in YbCH below 40 K. They gave the relation between $\tau_{Yb}$ and the temperature as

$$(\tau_{Yb})^{-1} = (1.0 \pm 0.1) \times 10^{-2} H^4 T + 0.47 \times 10^{-8} T^9 J_8 \qquad (3)$$

where

$$J_8 = \int_0^{\theta_D/T} [x^8 e^x / (e^x - 1)^2] \, dx \qquad (4)$$

with $\theta_D$ = 180 K, $x = \theta_D / T$, T is the upper temperature limit and H is the external field.

The values of $\tau_{Yb}$ calculated using equation (2) and equation (3) do not agree at all, but this can be explained by the fact that equation (2) is not valid below 180 K (Appendix 1). Mossbauer experiments by Kalvius et al.[5] above 30 K suggest a relation between temperature and $\tau_{Yb}$ as:

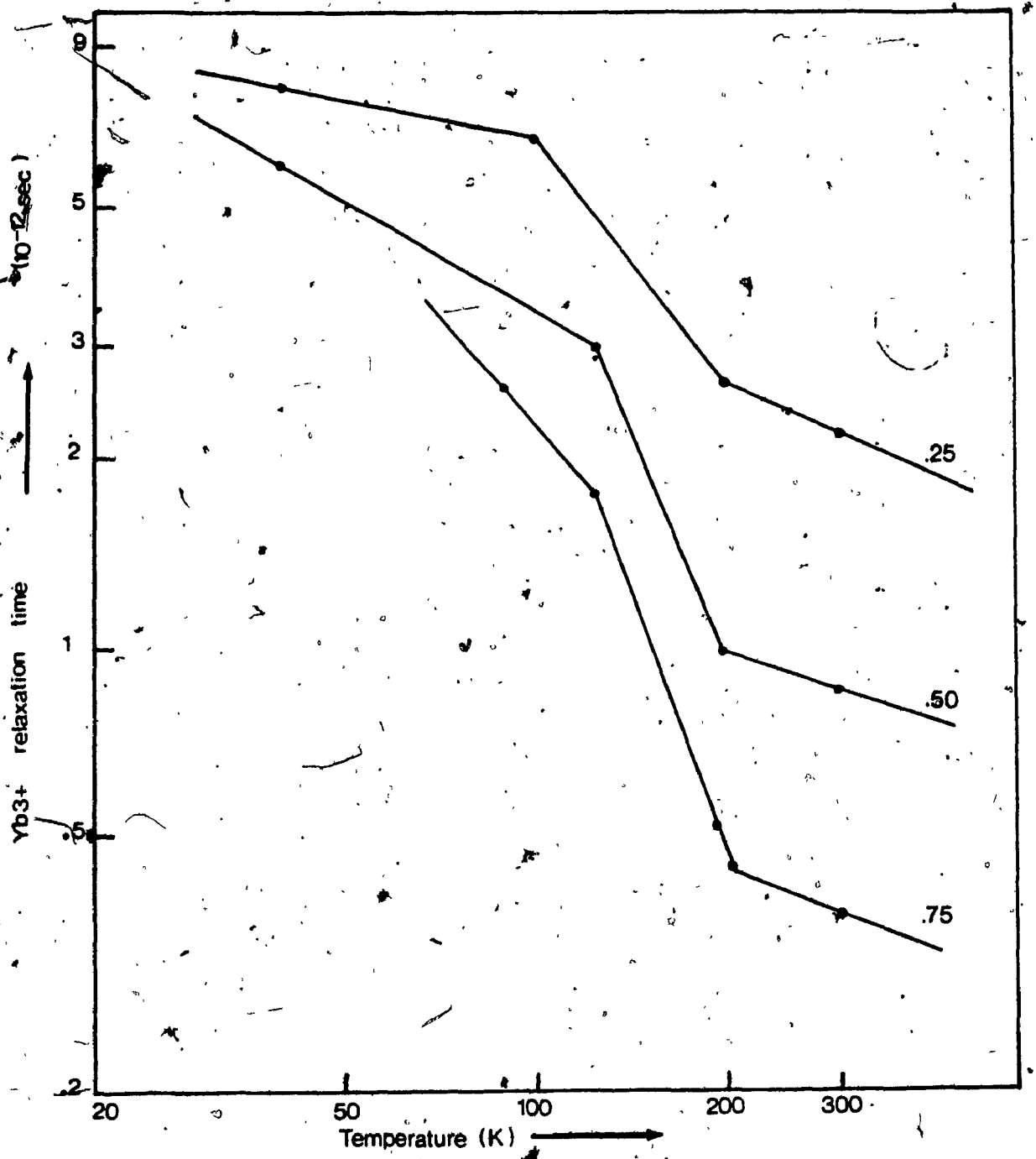


Figure 1: Log-log plot of $\tau_{Yb}$ vs. temperature for x=0.25, 0.50, 0.75, calculated using experimental $\Delta H_{1/2}$ results of Misra and Mikolajczak[3].

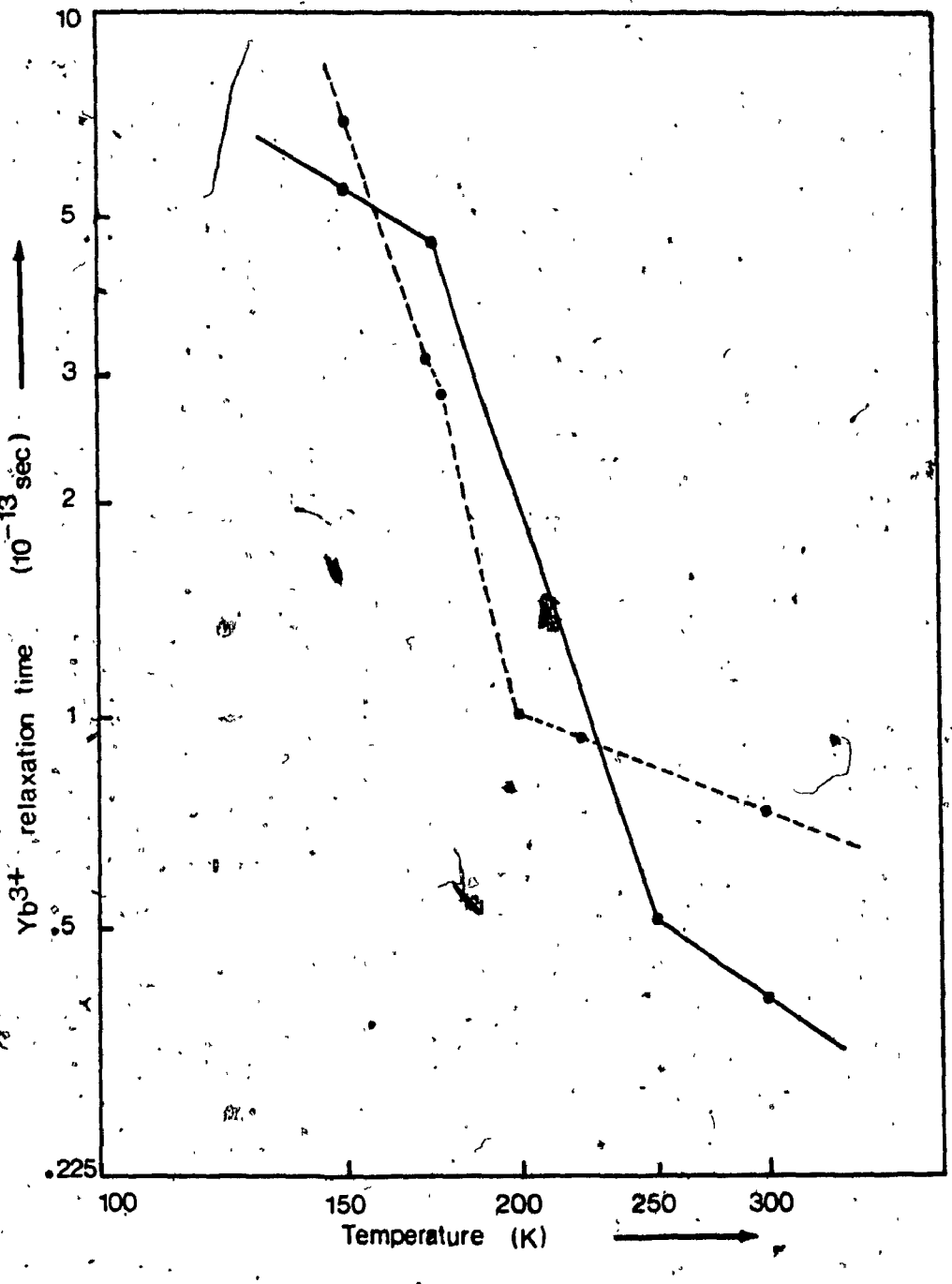


Figure 2: Log-log plot of $\tau^{*}_{Yb}$ vs. temperature for x=1.0 calculated using experimental $\Delta H_{1/2}$ values.(——):Malhotra et.al [2],(----):Misra and Sharp [1].

$$(\tau_{Yb})^{-1} = 4.8 \times 10^{11} \exp(-197/T) \qquad (5)$$

This relation gives longer spin-lattice relaxation times by a factor of 10 at 180 K and 50 at 300 K when compared to those calculated using eq.(2). Using eq.(5):

$$\tau_{Yb}\ (150\ K)/\tau_{Yb}\ (300\ K) = 1.92 \qquad (6)$$

Such a change in $\tau_{Yb}$ cannot explain the narrowing of $Gd^{3+}$ EPR linewidths as temperature goes up from 150 K to 300 K. Therefore, any equation giving $\tau_{Yb}$ as a function of temperature must be in agreement with Anderson's theory (and thus equation (2) ) so that the observed $Gd^{3+}$ linewidths can also be explained by spin-lattice relaxation narrowing, at least above 180 K.

Following Waller's theory on paramagnetic spin lattice relaxation, assuming that $\mu H \ll kT$, where $\mu$ and k are respectively the dipole moment and Boltzmann's constant, the following relation is obtained:

$$(\tau_{Yb})^{-1} = C \cdot S(S+1) T^7 \int_0^{\theta_D/T} [x^6 e^x/(e^x-1)^2]\, dx \qquad (7)$$

where C is a constant which depends on g, $\mu_B$, k, h, the speed of sound in the crystal, and the density of the crystal. C is estimated by Fierz[6] for some crystals but no value has been

| Temperature (K) | (i) ($10^{-4}$ T) | (ii) ($10^{-4}$ T) | (iii) ($10^{-4}$ T) |
|---|---|---|---|
| 297 | 16.5 | 29.0 | 13.2 |
| 258 | 19.0 | 34.0 | 18.0 |
| 240 | 20.0 | ——— | 20.0 |
| 220 | 23.0 | ——— | 24.0 |
| 180 | 30.5 | ——— | 37.0 |
| 170 | 36.0 | 50.0 | 42.0 |
| 150 | 70.0 | 58.6 | 55.0 |
| 126 | ——— | ——— | 75.0 |
| 90 | ——— | 144.0 | 179.0 |

Table 1: $Gd^{3+}$ EPR linewidths calculated using eq.(8) and observed experimentally.(i):Misra and Sharp[1],(ii):Malhotra et al.[2],(iii):calculated.

reported for YbCH. $\tau_{Yb}$ values obtained from equation (2) were used in equation (7) to calculate C and check if it remains constant for different temperatures. For YbCH in the temperature range 150-300 K, C was found to deviate 15% from its avarage value of $6.3\times10^{-4}$.

Combining eqs.(2) and (7) and solving for $\Delta H_{1/2}$, the following equation is obtained:

$$\Delta H_{1/2}=102(g\mu_B)^3 n^2\mu_o \Big/\Big\{3h\ 6.3\cdot10^{-4}\ T^7\int_0^{\theta_D/T}[x^6 e^x/(e^x-1)^2]dx\Big\} \quad (8)$$

where the value of C has been substituted into the equation. This equation gives theoretical linewidths, using theoretical spin—lattice relaxation times, in Anderson's theory of random modulation narrowing. Table 1 shows linewidths calculated using eq.(8) and linewidths observed experimentally by Misra and Sharp[1] and Malhotra et al.[2] for different temperatures.

$\Delta H_{1/2}$ values calculated using eq.(8) are closer to Misra and Sharp's[1] results in the range 180-300 K and seem to agree more with the results of Malhotra et al.[2] in the range 90-180 K.

# CHAPTER 3

## EPR LINEWIDTH

The magnetic resonance spectrum of an isolated atomic or nuclear moment consists of a single line at the Larmor frequency given by:

$$\nu_L = g\mu_B H/h \qquad (9)$$

where g, $\mu_B$, H, and h are respectively the g-factor, Bohr magneton, external magnetic field and Planck's constant. However when these moments are distributed on a crystal lattice, the dipolar interactions between neighboring paramagnetic ions cause a spread of the resonant frequency into a continuous band.

The resonance line is a result of the precession of the magnetic moment of the sample around the total external magnetic field vector. Thus magnetic interactions such as dipolar interactions, spin-orbit coupling or hyperfine interactions of nuclei and electrons will affect the resonant frequency. These interactions however are themselves affected by non-magnetic interactions such as the motion of atoms and electrons and motions in the spin system due to exchange or relaxation. These motions which cannot affect the line directly, produce the narrowing phenomenon.[7]

The dipolar interactions which cause the broadening of the resonance line will be considered first. This will be followed by the non-magnetic interactions which indirectly cause narrowing.

## 3.1 DIPOLAR BROADENING

Dipolar interactions, classified under "spin-spin" interactions, arise from the influence of the magnetic field of one paramagnetic ion on the neighboring paramagnetic ions. The total local field at any given site will depend on the arrangement of the neighbors and the directions of their dipole moments; the latter produce a distribution of the local field. In the presence of an external magnetic field, the local field at each ion must be added vectorially to it. If the local magnetic field is small compared to the external magnetic field, only the component of the local field parallel to the external magnetic field is important.[9] The size of this component varies from site to site, giving a random displacement to the resonant frequency of each ion which is similar in its effect to that due to inhomogeneity in the external magnetic field. For this reason this effect is also known as "inhomogeneous broadening". The shape of a line broadened by dipolar interactions cannot be readily computed; an assumption frequently made is that the shape is that of a Gaussian distribution. Van Vleck computed the

linewidths for various samples using the Gaussian assumption.[10] He found that in some cases the experimentally observed linewidths were narrower than those calculated theoretically.

## 3.2 NARROWING OF LINEWIDTH

Because of dipolar interactions the precession of the magnetic dipole about the external field will be frequency modulated. However, this modulation will be changing randomly due to the spin-lattice relaxation of the neighboring ions. This may reduce the effect of dipolar interactions and cause the narrowing phenomenon. This phenomenon was first discussed by Gorter and Van Vleck[11] and Van Vleck[10] in their exchange narrowing theories.

The sum of the Larmor frequencies which are due to the dipolar fields of the paramagnetic ions can be written as,

$$\nu_N(t)=\sum_{i=1}^{n}\nu_i(t) \tag{10}$$

and the resultant resonant frequency as

$$\nu_T(t)=\nu_L+\nu_N(t) \tag{11}$$

where the contribution of $\nu_N(t)$ to $\nu_T(t)$ will vary randomly. The smaller $\nu_N(t)$ becomes, the closer $\nu_T$ and $\nu_L$ will be;

thus the narrower the linewidths will be. If the spin-lattice relaxation is fast, the $\nu_i$'s will change sign many times in a time interval $\Delta t >> 1/\nu_i$ thus averaging out $\nu_N(t)$ to zero and making the deviation from $\nu_L$ smaller. Anderson and Weiss[12] and Kubo and Tomita[8] calculated the new linewidth affected by this random frequency modulation. The linewidth is given by:

$$\Delta H_{1/2} = 2(10/3)\Delta H_{dip}^2 / H_{mod} \qquad (12)$$

where $\Delta H_{dip}$ is due to dipolar interactions and is given by:

$$\Delta H_{dip}^2 = 5.1(g\mu_B n')^2 S(S+1) \qquad (13)$$

where $n'$ is the number of $Yb^{3+}$ ions per unit volume and S is the effective spin of $Yb^{3+}$ ions. Here $H_{mod}$ represents the modulating effects due to the spin-lattice relaxation process of neighboring ions and is given by:

$$H_{mod} = h/g\mu_B\tau \qquad (14)$$

where $\tau$ is the spin-lattice relaxation time of a neighboring ion. From equation (14) it is seen that as $\tau$ becomes smaller, $H_{mod}$ becomes larger thus making the linewidth $\Delta H_{1/2}$ smaller.

## 3.3 APPLICATION TO YbCH SINGLE CRYSTALS

Both the $Yb^{3+}$ and $Gd^{3+}$ ions are paramagnetic. As mentioned in Chapter 1, EPR experimental data on $Gd^{3+}$-doped YbCH single crystals indicate a temperature dependence of the $Gd^{3+}$ EPR linewidths. The dipolar interactions (spin-spin) cannot alone provide a full explanation of the observed linewidths, for two reasons: (i) Dipolar interactions are temperature independent and (ii) They, alone, give a much broader linewidth than that which was observed experimentally. Therefore these two reasons suggest a temperature-dependent narrowing mechanism.

Spin-lattice relaxation narrowing, also called modulation narrowing, has been invoked to explain the observed linewidths. This phenomenon was first proposed by Mitsuma[13], who suggested that the fast relaxation of host ions can randomly modulate the dipolar interactions between paramagnetic host ($Yb^{3+}$) and impurity ($Gd^{3+}$) ions in the same way as exchange interactions, as discussed by Anderson and Weiss.[12] Spin motions due to exchange interactions also cause narrowing of linewidths; however, this is temperature independent.

The applicability of Anderson and Weiss'[12] or Kubo and Tomita's[8] theory of exchange narrowing to the spin-lattice relaxation narrowing is discussed by Mitsuma[13]. The

conditions of applicability in the case of YbCH is discussed by Misra and Mikolajczak[3] and Malhotra et al.[2] These conditions are shown to be satisfied for YbCH in Appendix 1. Both Misra and Mikolajczak[3] and Malhotra et al.[2] used equations (12), (13), (14), which are based on the theory of spin-lattice relaxation narrowing, to calculate the $Yb^{3+}$ spin-lattice relaxation times using the experimentally observed linewidths.

# CHAPTER 4

## MAGNETIC RESONANCE

In this chapter the phenomenon of magnetic resonance in connection with the theory of the simulation will be discussed. The crystal structure and calculation of dipolar fields and Larmor frequencies due to host $Yb^{3+}$ ions will also be included.

### 4.1 THE PHENOMENON OF MAGNETIC RESONANCE

Classically a magnetic dipole experiences a torque in the presence of a magnetic field. It, thus, precesses about the magnetic field with a frequency given by eq.(9). To be consistent with EPR experiments this field is considered to be directed along the z-axis and designated by $H_z$. Another magnetic field rotating in the x-y plane, $H_1$, is now introduced. Using now a rotating coordinate axis x', y', z' having the same frequency $\nu$ as $H_1$, the effective field in the rotating coordinate system can be given as (figure 3):

$$H_e = H_1 i' + (H_z - \frac{\nu}{\gamma}) k' \qquad (15)$$

Here the gyromagnetic ratio $\gamma$ is defined as

$$\gamma = g\mu_B/h \qquad (16)$$

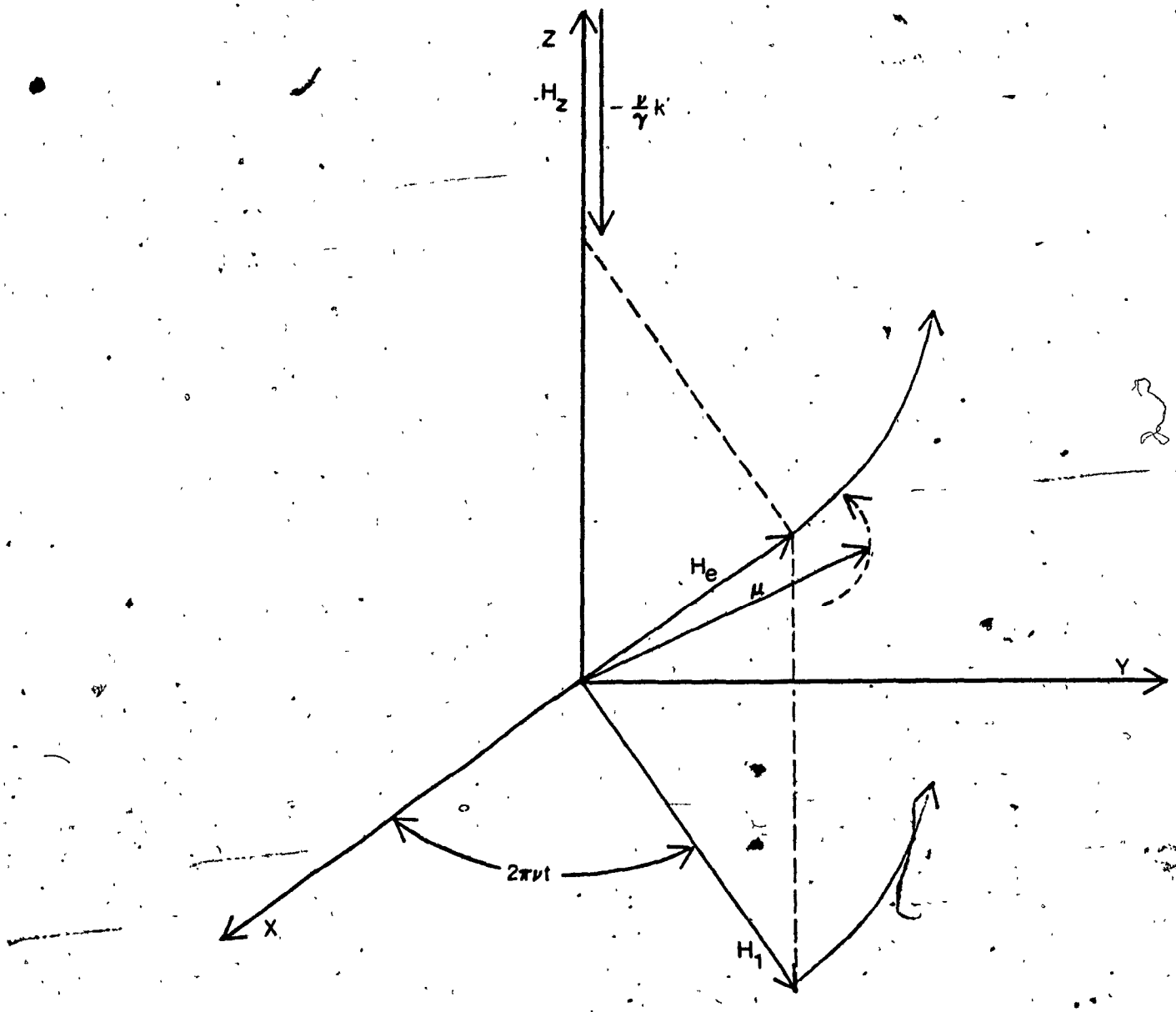


Figure 3. $H_1$ rotating in x-y plane, with the effective field $H_e$ rotating about the static external field $H_z$.

The magnetic dipole in this arrangement will rotate about $H_e$, while $H_e$ rotates about the static field $H_z$. The condition known as magnetic resonance occurs when:

$$H_z = \nu/\gamma \tag{17}$$

and hence:

$$H_e = H_1 \tag{18}$$

$H_e$ being perpendicular to $H_z$. Thus the magnetic dipole will precess about $H_1$ going from parallel to antiparallel to the z-axis. The locus of the end point of the magnetic moment is shown in figure 4. Thus the magnetic moment spirals down and back up repeatedly with a period T:

$$T = 1/\gamma H_1 \tag{19}$$

Note that for the geometry considered, a component of magnetization transverse to $H_z$ is obtained which will be designated as $M_T$. This transverse component itself has two components, one in phase with $H_1$ and the other 90° out of phase with $H_1$; these will be referred to as $M_x$ and $M_y$, respectively. They are frequently the components measured experimentally. The in-phase component leads to a susceptibility,

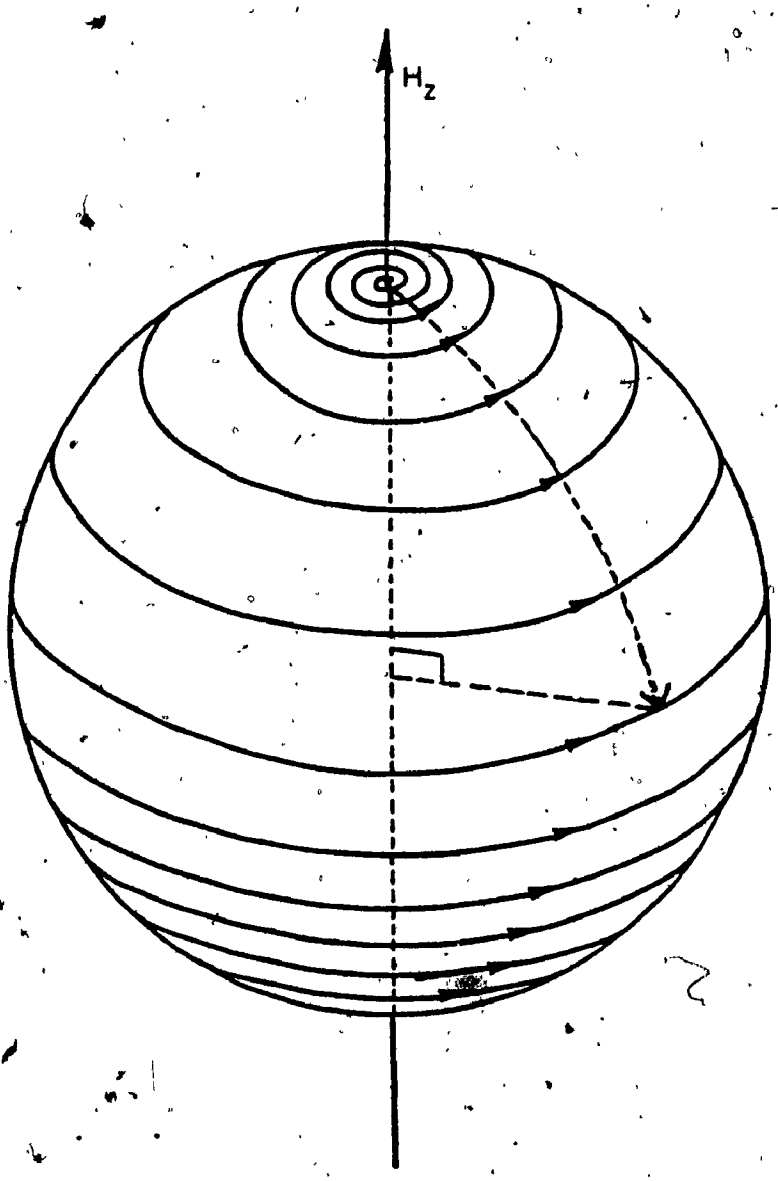


Figure 4: The path of the tip of magnetic moment vector at magnetic resonance. 90° degree pulse is also shown.

$$\chi' = M_x/H_1 \qquad (20)$$

which is called dispersion and the out of phase-component leads to another susceptibility,

$$\chi'' = -M_y/H_1 \qquad (21)$$

which is called absorption.

If magnetization is at its thermal equilibrium value, $M_o = M_z = \chi_z H_z$ and one allows $H_1$ to be turned on for a time $1/4\gamma H_1$ only, and if $\nu = \gamma H_z$, then after the 90° pulse (as it is called) (fig.4), the magnetization will be precessing at the Larmor frequency in the x-y plane. This precession will eventually decay exponentially due to relaxation and the magnetization will approach its thermal equilibrium value $M_o$. The transverse magnetization components $M_x$ and $M_y$ are shown in figure 5. Note that two factors can now affect $M_y$: (i) The exponential decay of M, and (ii) Changes in $H_z$ (such as due to the effects of neighboring dipolar fields). If there were no changes in $H_z$, the angle $\phi$ between $M_T$ and x'-axis would remain constant since both would be rotating at the same frequency. However any change in $H_z$ would cause a deviation from the Larmor frequency which can be represented by a phase deviation. As can be seen from fig.5, any change of $\phi$ would cause a change

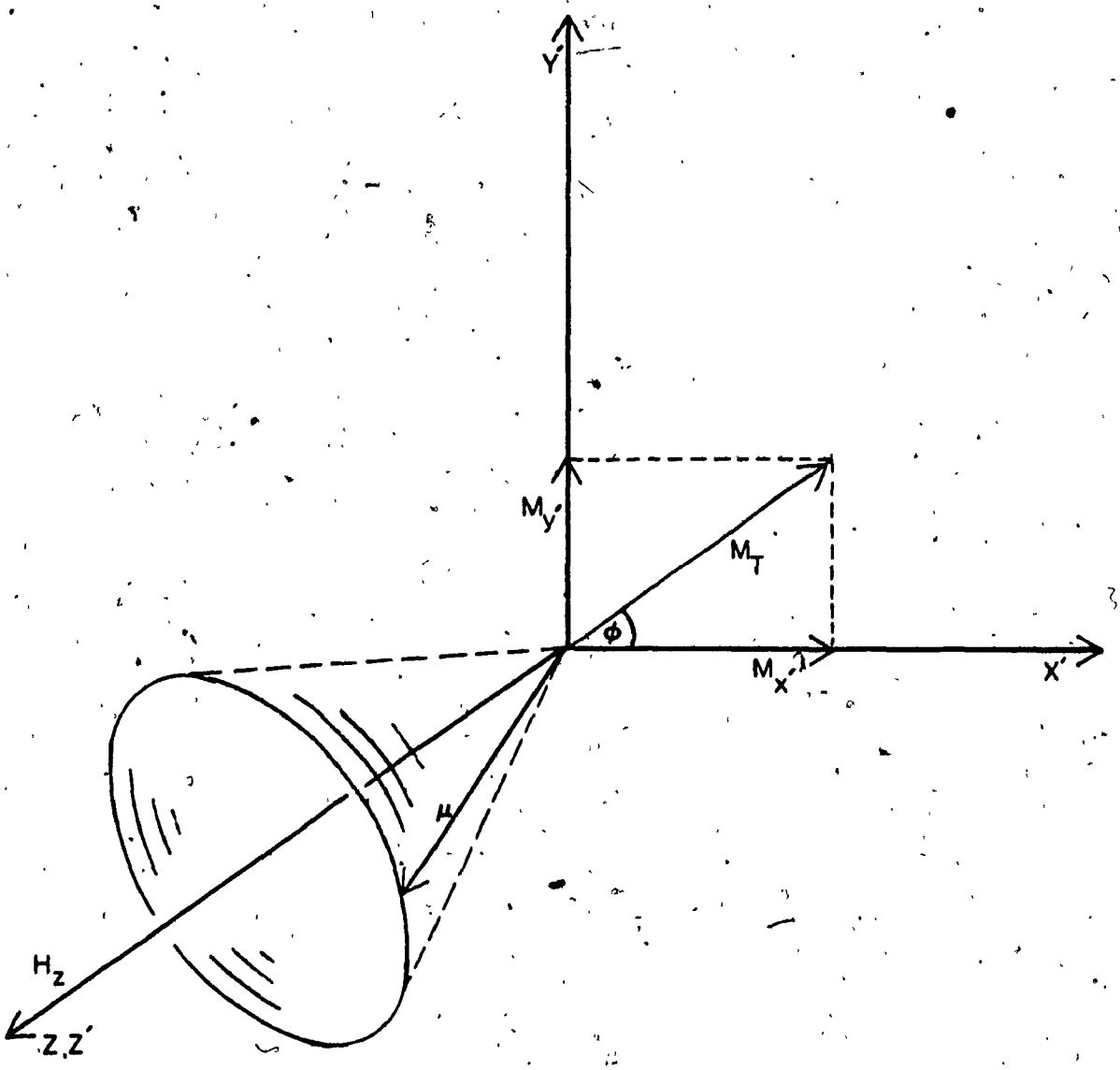


**Figure 5: The transverse magnetization $M_T$ and its components $M_{x'}$ and $M_{y'}$.**

in $M_y$. Considering many sites like this each with different deviations of $H_z$, different values of absorption would result for different sites thus giving a broadened resonance line. However if these changes in $H_z$ are fast enough their broadening effect may be reduced, thus a narrowing of the "broadened" line would result.

From figure 5 it can be shown that:

$$M_T = M_y \sin\phi + M_x \cos\phi \tag{22}$$

and,

$$M_y = M_T \sin\phi \tag{23}$$

Furthermore, defining $\nu_N$ as the sum of Larmor frequencies due to the dipolar fields which cause the changes in $H_z$, thus

$$\nu_N(t) = \sum_{i=1}^{N} \nu_i(t) \tag{24}$$

Using (22) the following relation can be derived:

$$dM_T/dt = -\nu_N M_z \sin\phi \tag{25}$$

Derivation of (25) is given in Appendix 2. Equation (25) can be integrated leading to:

$$M_{T_2} = M_{T_1} - \frac{\nu_N M_z}{\nu_L + \nu_N}(\cos\phi_1 - \cos\phi_2) \qquad (26)$$

where subscripts 2 and 1 indicate the upper and lower limits of integration. The equations (23) and (26) can be written, in equivalent forms as

$$H_y = H_T \sin\phi \qquad (27)$$

and,

$$H_{T_2} = H_{T_1} - \frac{\nu_N H_z}{\nu_L + \nu_N}(\cos\phi_1 - \cos\phi_2) \qquad (28)$$

Defining the sum of the Larmor frequency due to $H_z$ and the Larmor frequencies due to dipolar fields by

$$\nu_T(t) = \nu_L + \sum_{i=1}^{N} \nu_i(t) \quad , \qquad (29)$$

the phase angle, assuming that the precession is decaying exponentially , can be written as

$$\phi(t') = \int_0^{t'} \nu_T(t) e^{-t/\tau}\, dt \qquad (30)$$

where $\tau$ is the relaxation time of the magnetic dipole, and $t' \ll \tau$.

## 4.2 THE CRYSTAL STRUCTURE OF $Yb_x Y_{1-x}$CH SINGLE CRYSTALS

In order to calculate $Yb^{3+}$ ion dipolar fields at $Gd^{3+}$ site, its crystal structure has to be taken into account. The crystal structure for all the rare-earth trichloride hexahydrates is monoclinic; there are two molecules per unit cell and each rare-earth ion is surrounded by two chlorine and six water molecules. Unit cell parameters for YbCH are: a=0.953 nm, b=0.643 nm, c=0.780 nm ,$\beta$=93° 40'. From these values it is also possible to estimate the unit cell parameters for $Yb_x Y_{1-x}$CH crystals using Vegard's law, according to which the lattice parameters of primary solid solutions vary nearly linearly with the atomic percentage of the solute element. For $Yb_{0.5} Y_{0.5}$CH the following parameters are found : a=0.956 nm, b=0.646 nm, c=0.783 nm, $\beta$=93 40' . Coordinates of rare-earth ions are: $\pm$(0.25, 0.1521, 0.25)[15]. Using these and the unit cell parameters distances between rare-earth ions can be calculated. Calculation of these distances indicates that each impurity ion ($Gd^{3+}$) has two nearest, four second nearest and four third nearest neighbors. The distances of $Yb^{3+}$ ions to the $Gd^{3+}$ ion are: $r_1$=0.643 nm, $r_2$=0.646 nm, $r_3$=0.761 nm and their positions with respect to the $Gd^{3+}$ ion are shown in fig. 6.

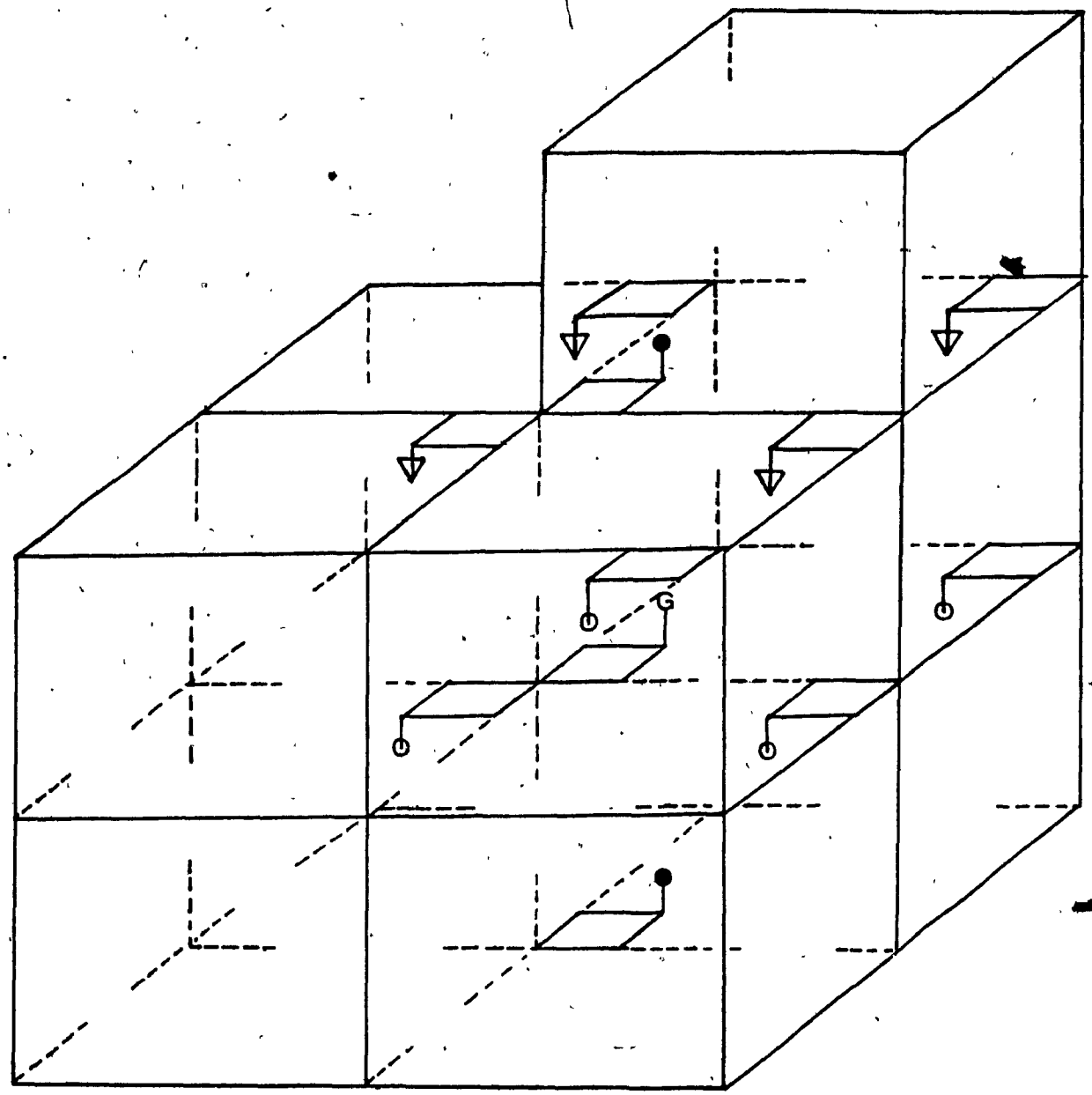

Figure 6: Nearest, second nearest, and third nearest neighbors of $Gd^{3+}$ ion in YbCH.G:Gd , ●: nearest, O: $2^{nd}$ nearest, $\nabla$:$3^{rd}$ nearest.

| Neighbor ($Yb^{3+}$) | | $r_i$ | $z_i$ | $Gd^{3+}$ Larmor frequency |
|---|---|---|---|---|
| | (i) | (nm) | (nm) | (Hz) |
| Nearest | 1 | 0.643 | 0.0 | $-4.4069 \times 10^8$ |
| | 2 | 0.643 | 0.0 | $-4.4069 \times 10^8$ |
| $2^{nd}$ Nearest | 3 | 0.646 | -0.390 | $+4.0595 \times 10^7$ |
| | 4 | 0.646 | +0.390 | $+4.0595 \times 10^7$ |
| | 5 | 0.646 | -0.390 | $+4.0595 \times 10^7$ |
| | 6 | 0.646 | -0.390 | $+4.0595 \times 10^7$ |
| $3^{rd}$ Nearest | 7 | 0.761 | +0.390 | $-5.6379 \times 10^7$ |
| | 8 | 0.761 | +0.390 | $-5.6379 \times 10^7$ |
| | 9 | 0.761 | -0.390 | $-5.6379 \times 10^7$ |
| | 10 | 0.761 | -0.390 | $-5.6379 \times 10^7$ |

Table 2: Ten nearest neighbors of $Gd^{3+}$ their distances $r_i$, z-coordinate of $Gd^{3+}$, and $Gd^{3+}$ Larmor frequencies.

## 4.3 CALCULATION OF DIPOLAR FIELDS AND LARMOR FREQUENCIES

The z-component of the magnetic field due to a dipole at the origin of a Cartesian coordinate system is given as:

$$H = \frac{\mu_0 \mu}{4\pi}\left(-\frac{1}{r^3} + \frac{3z^2}{r^5}\right) \qquad (31)$$

where r is the distance between $Gd^{3+}$ and $Yb^{3+}$ ions, z is the z-coordinate of $Gd^{3+}$ ion ($Yb^{3+}$ placed at the origin), $\mu_0$ is the permability constant and $\mu$ is the magnetic moment of $Yb^{3+}$ ion given as:

$$\mu = g\mu_B[S(S+1)]^{1/2} \qquad (32)$$

with S being the effective spin of $Yb^{3+}$ ion. At temperatures T<30 K ,S=1/2 and in the temperature range 30<T<180, S=3/2. Above 180K the effective spin of $Yb^{3+}$ ion is S=5/2 and this value of S is used in the simulation for the temperature range 180 K<T<300 K.

After calculation of $H_z$ values for ten neighboring $Yb^{3+}$ ions corresponding Larmor frequencies $\mu_i$ of $Gd^{3+}$ are calculated using eq.(9), these are given in Table 2.

# CHAPTER 5

## MONTE CARLO COMPUTER SIMULATION

The purpose of the computer simulation is to find the phase angle $\phi(t)$ between $M_T$ and $M_x$ (fig.5). This angle will vary randomly with time due to random relaxations of neighboring $Yb^{3+}$ ions. The randomness of the relaxation process is achieved in the computer simulation by means of the Monte Carlo method. Once $\phi(t)$ is found, $H_y$ can be calculated using eqs.(28) and (27) : These calculations are performed many times for different $Gd^{3+}$ sites. At each $Gd^{3+}$ site a different value of $\phi(t)$ is expected since the neighboring $Yb^{3+}$ ions relax randomly with time, thus giving different $H_y$ values as well. Therefore a histogram of many $H_y$ values would represent the absorption not of a single moment but of the lattice.

### 5.1 PHYSICAL PICTURE OF CALCULATION

Following the 90° pulse, the $Gd^{3+}$ magnetic dipole precesses in the x-y plane due to the external field $H_z$ with the Larmor frequency $\nu_L$ . This precession will decay exponentially and the magnetization will approach its equilibrium value due to the $Gd^{3+}$ spin-lattice relaxation. During this decay, the spin flips of the neighboring $Yb^{3+}$ ions, due to their spin-lattice relaxation, will cause

changes in the local field at the $Gd^{3+}$ site thus modifying correspondingly the precession frequency of the $Gd^{3+}$ dipole moment and the angle $\phi$. The spin-lattice relaxation of the $Gd^{3+}$ ion can be divided into small time intervals and after each interval, the time elapsed from the beginning of the decay can be compared with the spin-lattice relaxation times of the $Yb^{3+}$ ions. If the time elapsed from the beginning is greater than the spin-lattice relaxation time of any $Yb^{3+}$ ion, its contribution to the precession frequency of the $Gd^{3+}$ dipole moment will reverse sign as it flips, because of the reversal of the direction of its dipolar field at the $Gd^{3+}$ site. The spin flips of $Yb^{3+}$ ions are simulated by choosing random numbers, Gaussian distributed around $Yb^{3+}$ spin-lattice relaxation time. This calculation is repeated for each time interval for all the $Yb^{3+}$ ions until the $Gd^{3+}$ ion has decayed, with a spin-lattice relaxation time determined by $\propto (\tau_{Gd}/\tau_{Yb})$, which is input to the program. The resulting $\phi$ and $H_y$ values are used to calculate the EPR linewidths of $Gd^{3+}$ ion, by considering a large number of $Gd^{3+}$ sites and plotting a histogram of $H_y$ values.

## 5.2 EXPLANATION OF THE PROGRAM

One thousand $Gd^{3+}$ sites, each with ten neighboring $Yb^{3+}$ ions, were considered in the computer program. These ten $Yb^{3+}$ neighbors are two nearest, four second nearest and four third nearest neighbors. The Larmor frequency of $Gd^{3+}$ ion

due to the external magnetic field $H_z$ is calculated using $g_z(Gd^3)=1.981$. The $Gd^{3+}$ Larmor frequencies due to $Yb^{3+}$ ions, which were calculated in Chapter 4 are input to the program. The spin-lattice relaxation time ratio $\alpha$, is a variable and can be varied to simulate temperature changes.

The procedure for one $Gd^{3+}$ site is as follows: Ten random numbers between 0 and 1 are generated using a suitable subroutine (RANF) and the closest integer is calculated, giving only 0's and 1's. If the random integer is a zero, then the corresponding $Yb^{3+}$ ion is set "down", and "up" if the random integer is a one. Next, another subroutine (GGNML) is used to generate Gaussian distributed random numbers, which are converted to random relaxation times about a mean spin-lattice relaxation time. For a short interval of time $\Delta t$, $d\phi$ is calculated using

$$d\phi = \nu_T(t)\exp(-t/\tau_{Gd})\Delta t \qquad (33)$$

where $\Delta t$ was chosen 100 times smaller than the $Yb^{3+}$ mean spin-lattice relaxation time and $\nu_T(t)$ is given by eq.(29).

Calculations are made for successive time intervals and the sum of the phase angles is given as

$$\sum_{j=1}^{N} d\phi_j = \sum_{j=1}^{N} \nu_{T_j} \exp(-j\Delta t/\tau_{Gd})\,\Delta t \qquad (34)$$

The largest value of the ten relaxation times is found, which is designated by $\tau_m$, and N in (34) is calculated using:

$$N=\tau_m/\Delta t \qquad (35)$$

In each step of the summation, the spin-lattice relaxation times of $Yb^{3+}$ ions are compared with the time elapsed and if $\tau_i$ of any neighbor has expired, the sign of the corresponding $\nu_i$ in eq.(29) will be changed. Since, $N\Delta t=\tau_m$, at the end of time $N\Delta t$ all of the neighbors will have "flipped" at least once depending on the relaxation time.

After the summation is finished another set of ten random relaxation times will be assigned to the neighbors and the same precedure is repeated until the $Gd^{3+}$ ion decays, thus,

$$\tau_{Gd}=\sum_{i=1}^{n} N_i\Delta t \qquad (36)$$

Both $\phi(t)$ and $H_T$ (eq.28) values are accumulated during the $Gd^{3+}$ decay. Thus, after a time $\tau_{Gd}$ using final values of $\phi(t)$ and $H_T$, one can calculate $H_y$, corresponding to one $Gd^{3+}$ site, using eq.(27). Since, $\tau_m$ is different for each set of 10 relaxation times, N will be also different for each summation, thus making n different for each $Gd^{3+}$ site.

The whole precedure can be repeated one thousand times for a preset relaxation time ratio $\alpha$ ($= \tau_{Gd}/\tau_{Yb}$), giving at the end one thousand $H_y$ values. The listing and the flowchart of the program are given in Appendix 3.

## 5.3 CASE OF $Yb_{0.5}Y_{0.5}CH$ CRYSTALS

In the case of the $Yb_{0.5}Y_{0.5}CH$ crystal, half of the paramagnetic $Yb^{3+}$ ions are replaced by the diamagnetic $Y^{3+}$ ions. Therefore a new arrangement of the neighbors is required for the simulation. However, there seems to be no information on, where in the unit cell, the $Y^{3+}$ ion would go. Another possibility is that the $Yb_{0.5}Y_{0.5}CH$ crystal would be formed as a mixture of YbCH and YCH ($YCl_3 \cdot 6H_2O$) unit cells. Vegard's law dictates how the YbCH unit cell would expand with the insertion of $Y^{3+}$ ions, but from this information the exact location of the $Y^{3+}$ ions cannot be determined.

In the case of alternating YCH and YbCH unit cells, there are two possible locations for the $Gd^{3+}$ ion. These two possible configurations are shown in fig.7. The distances of nearest neighbors are different in both cases. Also in the case of alternating ions in the unit cell, there are two possible locations for the $Gd^{3+}$ ion and these configurations are shown in fig.8. These four possible configurations are designated by the letters A, B, C, and D respectively.

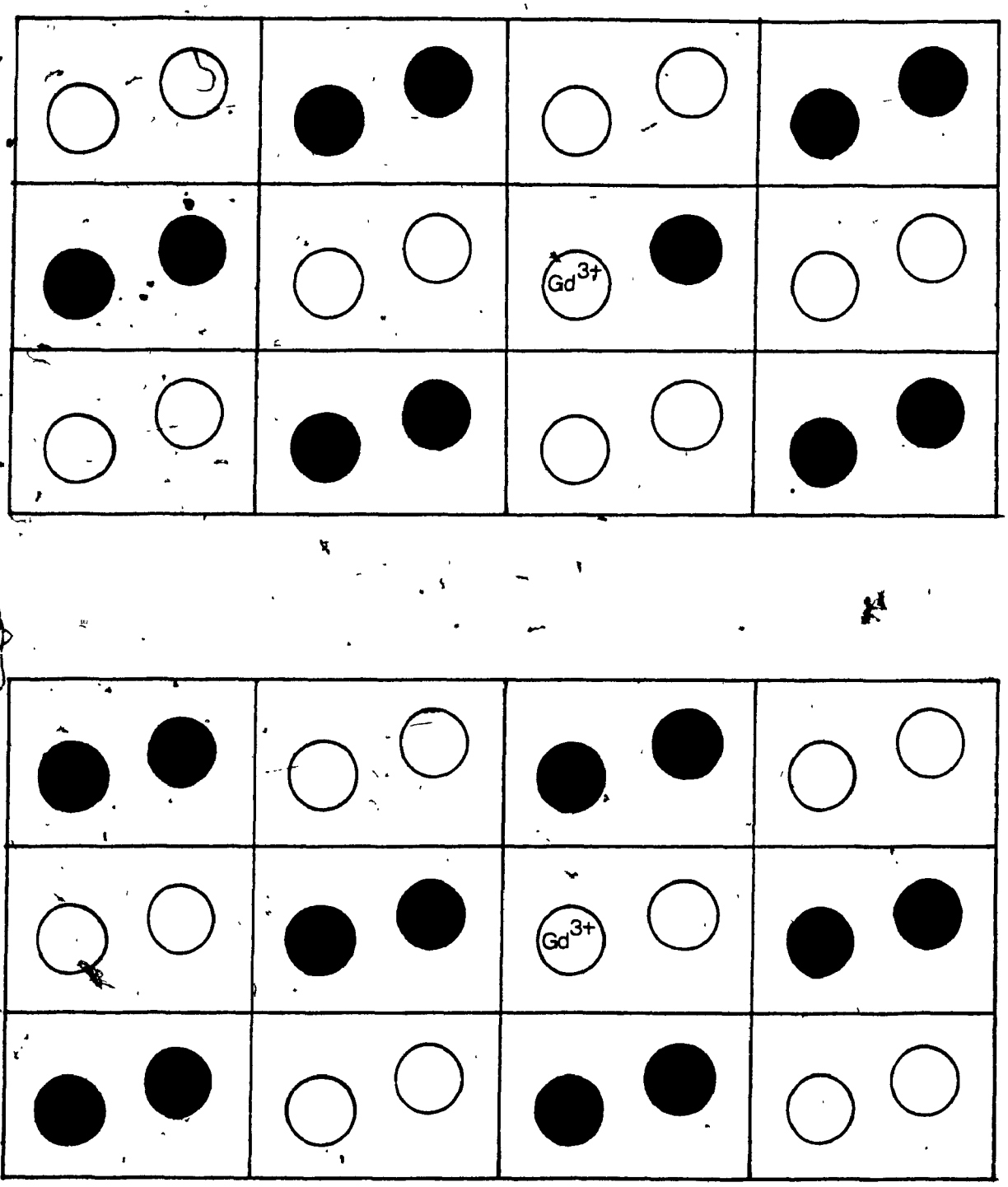


Figure 7: Two possible configurations A (top) and B (bottom) in the case of alternating unit cells. O: $Yb^{3+}$, ●: $Y^{3+}$.

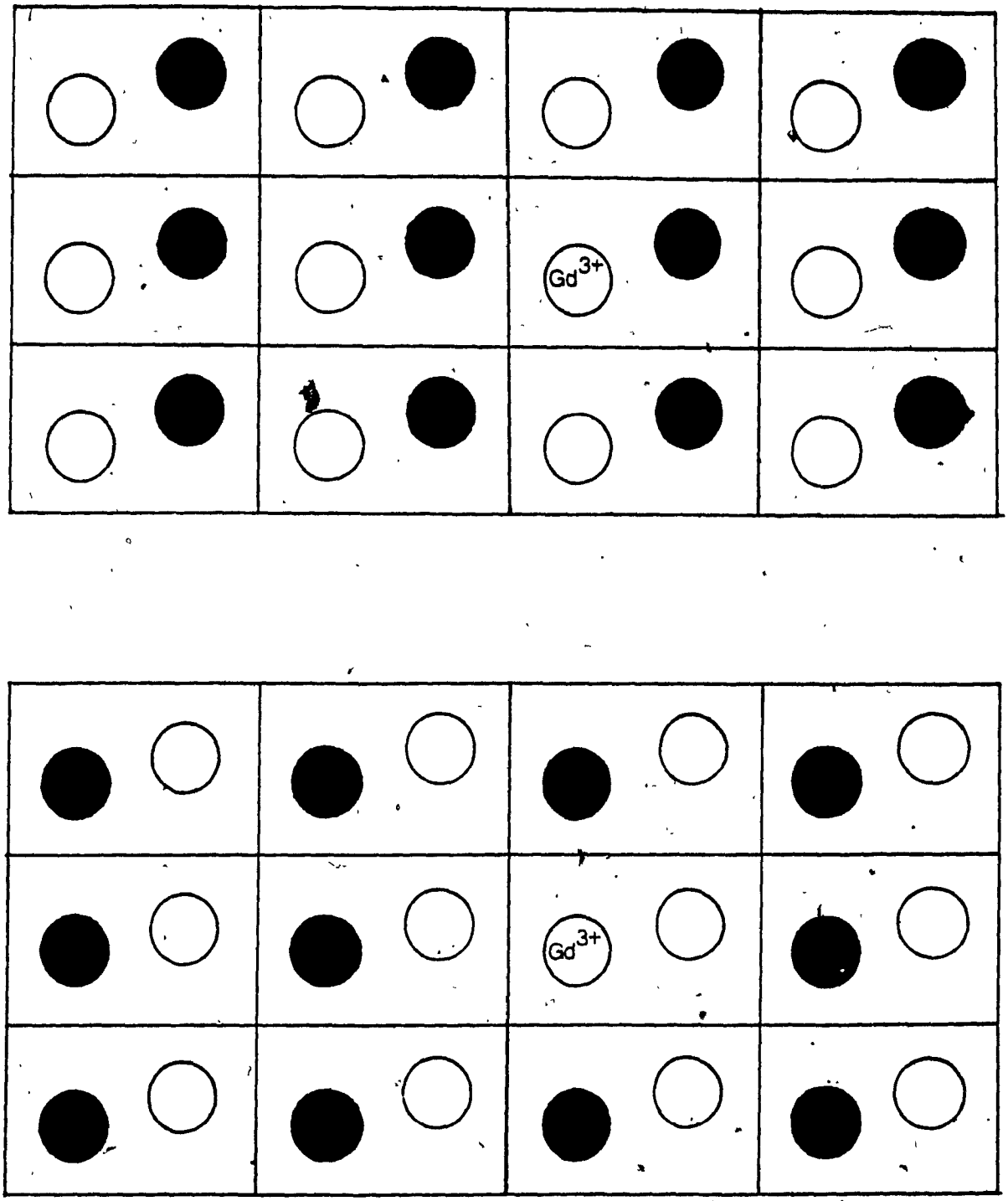


Figure 8: Two possible configurations D (top) and C (bottom) in the case of alternating ions in the unit cell. O :$Yb^{3+}$, ●: $Y^{3+}$.

| | Neighbor i-j | $r_{ij}$ (nm) | $z_{ij}$ (nm) | $\nu_{ij}$ ($Gd^{3+}$) (Hz) |
|---|---|---|---|---|
| Config.A | 1-1 | 0.643 | 0.0 | $-4.4069 \times 10^{8}$ |
| | 1-2 | 0.643 | 0.0 | $-4.4069 \times 10^{8}$ |
| | 2-1 | 0.646 | -.390 | $+4.0595 \times 10^{7}$ |
| | 2-2 | 0.646 | +.390 | $+4.0595 \times 10^{7}$ |
| Config.B | 1-1 | 0.646 | -.390 | $+4.0595 \times 10^{7}$ |
| | 1-2 | 0.646 | +.390 | $+4.0595 \times 10^{7}$ |
| | 2-1 | 0.761 | -.390 | $-5.6379 \times 10^{7}$ |
| | 2-2 | 0.761 | +.390 | $-5.6379 \times 10^{7}$ |
| Config.C | 1-1 | 0.646 | +.390 | $+4.0595 \times 10^{7}$ |
| | 1-2 | 0.646 | +.390 | $+4.0595 \times 10^{7}$ |
| | 1-3 | 0.646 | -.390 | $+4.0595 \times 10^{7}$ |
| | 1-4 | 0.646 | -.390 | $+4.0595 \times 10^{7}$ |
| | 2-1 | 0.761 | +.390 | $-5.6379 \times 10^{7}$ |
| | 2-2 | 0.761 | +.390 | $-5.6379 \times 10^{7}$ |
| | 2-3 | 0.761 | -.390 | $-5.6379 \times 10^{7}$ |
| | 2-4 | 0.761 | -.390 | $-5.6379 \times 10^{7}$ |
| Config.D | 1-1 | 0.643 | 0.0 | $-4.4069 \times 10^{8}$ |
| | 1-2 | 0.643 | 0.0 | $-4.4069 \times 10^{8}$ |

Table 3: $Yb^{3+}$ neighbors, in $Yb_{0.5}Y_{0.5}CH$ for the four configurations, their distances $r_{ij}$, z-coordinate of $Gd^{3+}$, and $Gd^{3+}$ Larmor frequencies.

The computer program can be modified for any of these four cases, by using the appropriate number of neighbors and their corresponding $\nu_i$ . Table 3 gives the number of neighbors, their distances $r_{ij}$ and corresponding Larmor frequencies $\nu_{ij}$ .

# CHAPTER 6

## THEORETICAL RESULTS AND COMPARISON WITH EXPERIMENTAL DATA

In this chapter, the results of a computer simulation for both cases, YbCH and $Yb_{0.5}Y_{0.5}CH$, will be given. Also, the experimental results will be compared with the theoretical values.

### 6.1 RESULTS OF MONTE CARLO SIMULATION FOR YbCH

The computer program was run for the following values of $\alpha$ ($\tau_{Gd}/\tau_{Yb}$): 1.2, 3, 10, 25, 50, 75, 100, 200, 400, and 800 for the YbCH case. $\alpha<1$ is not considered since (even at very low temperatures) $\tau_{Yb}<\tau_{Gd}$, thus $\alpha>1$. Ratios higher than 800 can be considered, but very long computing times are required ($\alpha$=800 takes approx. 32000 cpu seconds). The external field $H_z$ of ($3000\times10^{-4}$ Teslas) was used in eq.(28). The $H_y$ values are calculated using eq.(27). The histograms of these values were plotted for each value of $\alpha$. Each histogram has twenty-five intervals each with forty values. All histograms have the shape of a Gaussian distribution. The linewidths $\Delta H_{1/2}$, at half of the peak value were measured. $\Delta H_{1/2}$ values for each $\alpha$ value are shown in Table 4. The histograms for $\alpha$=3, 75, 100 are given in fig.9 and for $\alpha$=200, 400, 800 in fig.10. Log-log plots of $\Delta H_{1/2}$ vs. $\alpha$ for $\alpha<100$ and $\alpha\geq100$ are also shown in figs.11 and 14 respectively.

| Relaxation time ratio $\alpha$ | $Gd^{3+}$ Linewidth ($10^{-4}$ T) |
|---|---|
| 1.2 | 12.99 |
| 3.0 | 22.00 |
| 10.0 | 37.79 |
| 25.0 | 35.00 |
| 50.0 | 32.28 |
| 75.0 | 32.20 |
| 100.0 | 43.30 |
| 200.0 | 33.80 |
| 400.0 | 29.00 |
| 800.0 | 22.00 |

Table 4: Simulated $Gd^{3+}$ EPR linewidths for $\alpha$=1.2-800 for YbCH.

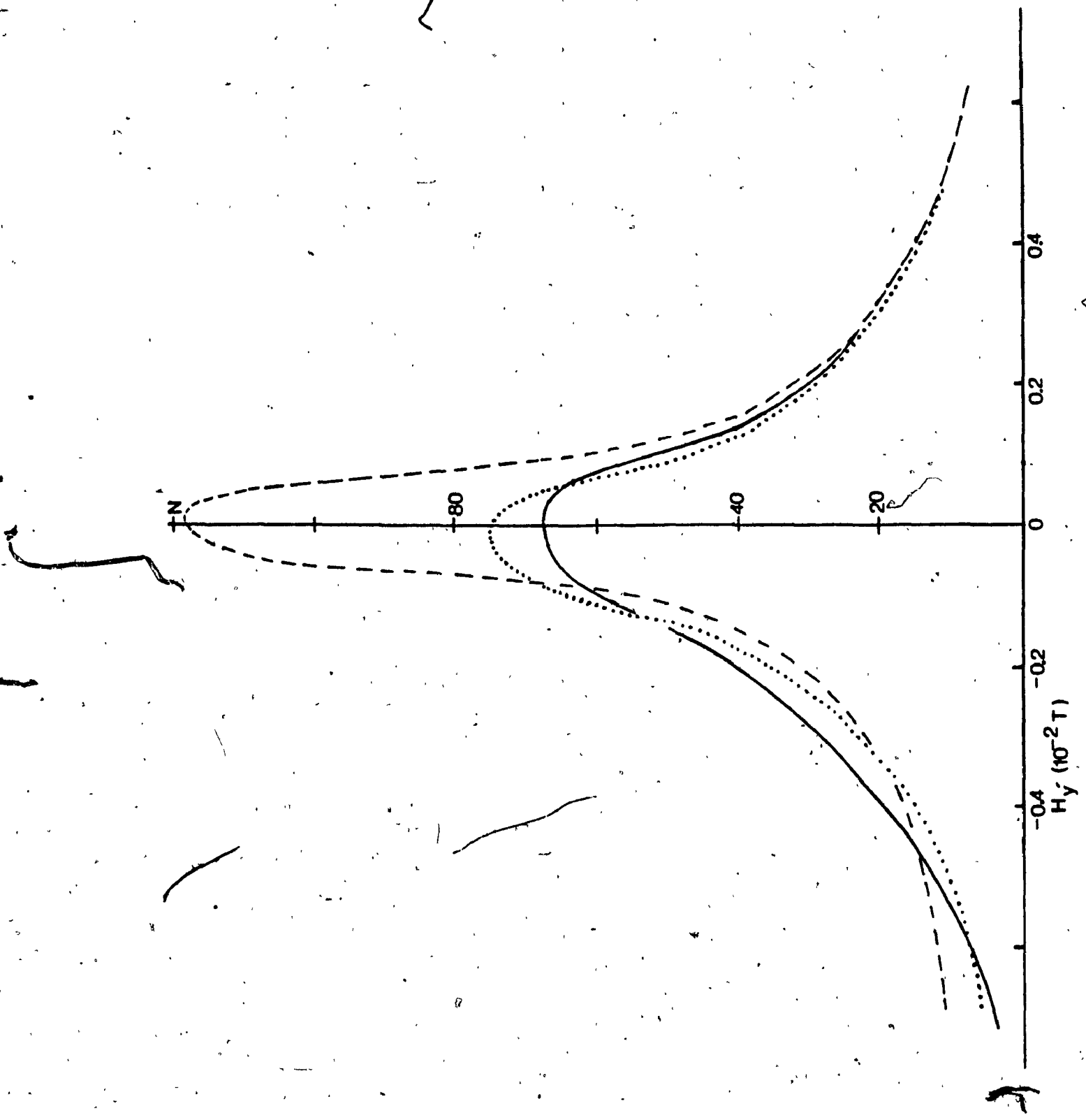


Figure 9: The historams of $H_y$ for $\alpha$=3, 75, 100 in YbCH. (-·-):3, (---):75, (—):100.

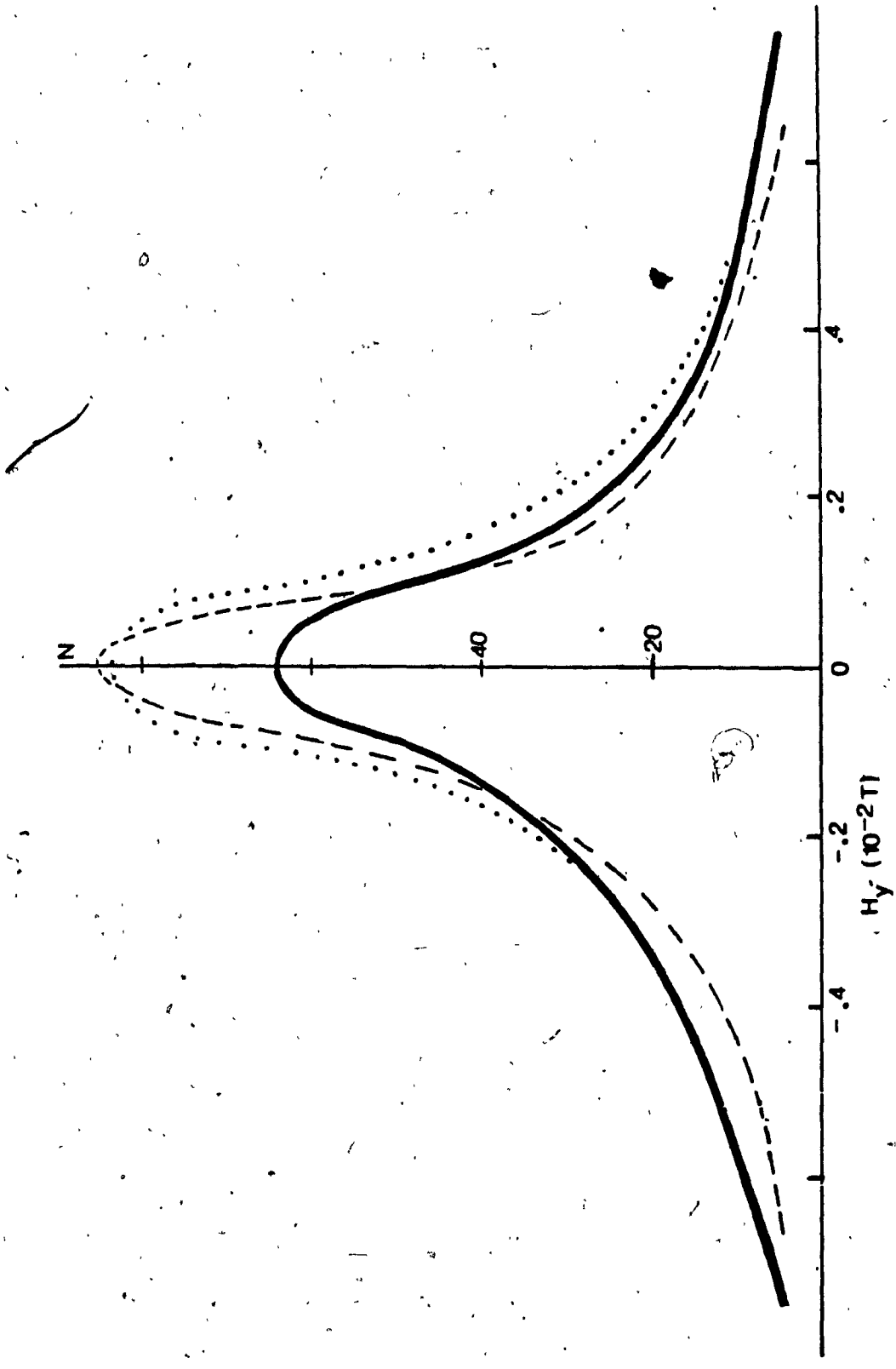


Figure 10: The histograms of $H_y$ for $\alpha$=200, 400, 800 in YbCH. (—):200, (---):400, (— —):800.

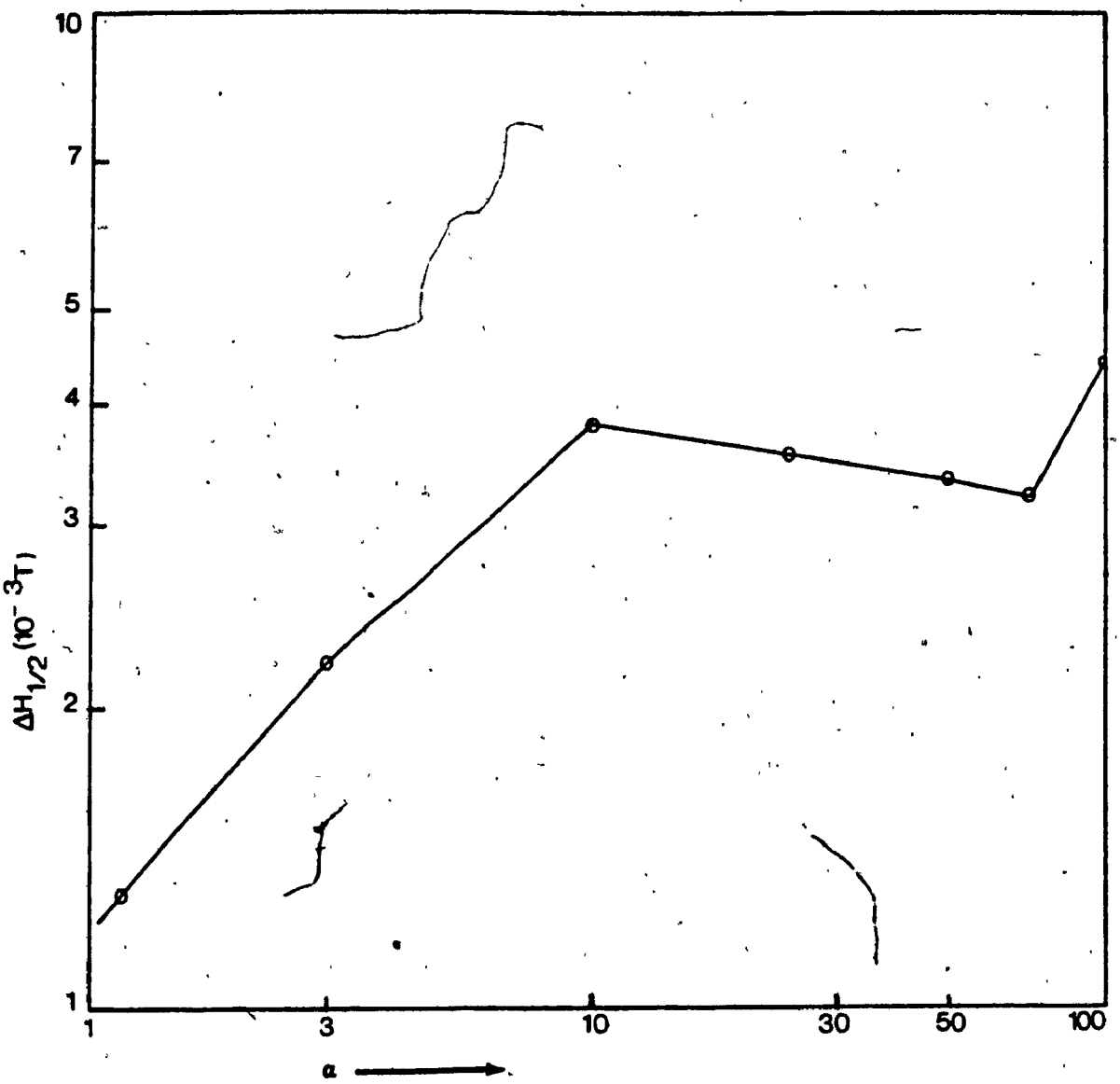


Figure 11: Log-log plot of linewidth vs. relaxation time ratio $\alpha \leq 100$ in YbCH.

## 6.2 RESULTS FOR $Yb_{0.5}Y_{0.5}CH$

The histograms for $Yb_{0.5}Y_{0.5}CH$ are plotted for $\alpha$=1.2, 5, 10, 50, 100, 200 and 400 in the same way as for YbCH. These ratios were repeated for configurations A, B, C, and D (Chapter 5). Also a sum of four configurations is calculated for each $\alpha$ value. Log-log plots of $\Delta H_{1/2}$ vs. $\alpha$ are given for $\alpha \leq 100$ and for $\alpha \geq 100$ in figs.12 and 13 respectively for the four configurations as well as their sum.

## 6.3 RESULTS OF EPR EXPERIMENTS

The $Gd^{3+}$ linewidths in YbCH observed by Misra and Sharp[1] and by Malhotra et.al[2] in the temperature range 90-300 K are given in Table 1. Log $\Delta H_{1/2}$ is also plotted versus temperature in the 170-300 K range (fig.14). For the $Yb_{0.5}Y_{0.5}CH$ case log of $Gd^{3+}$ linewidths observed by Misra and Mikolajzcak[3] are plotted versus temperature in the 170-300 K range (fig.15).

## 6.4 COMPARISON OF THEORETICAL AND EXPERIMENTAL RESULTS FOR YbCH

The theoretical linewidths show a narrowing as $\alpha$ goes down from 10 to 1.2 . Since the ratio $\alpha$ is expected to

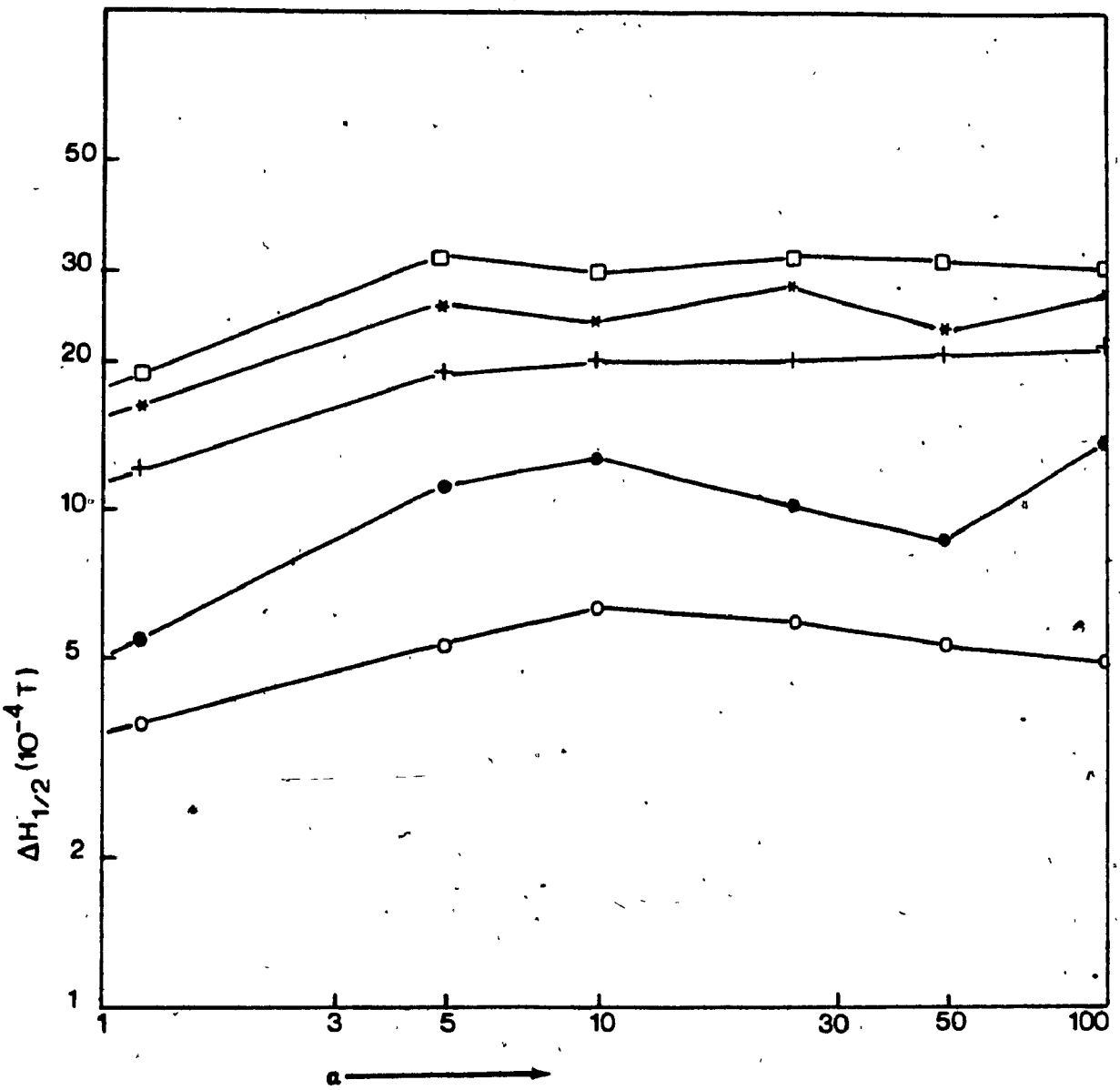


Figure 12: Log $\Delta H_{1/2}$ vs. log $\alpha$, for $\alpha \leq 100$ in $Yb_{0.5}Y_{0.5}CH$. A:□, B:o, C:●, D:*, Sum:+.

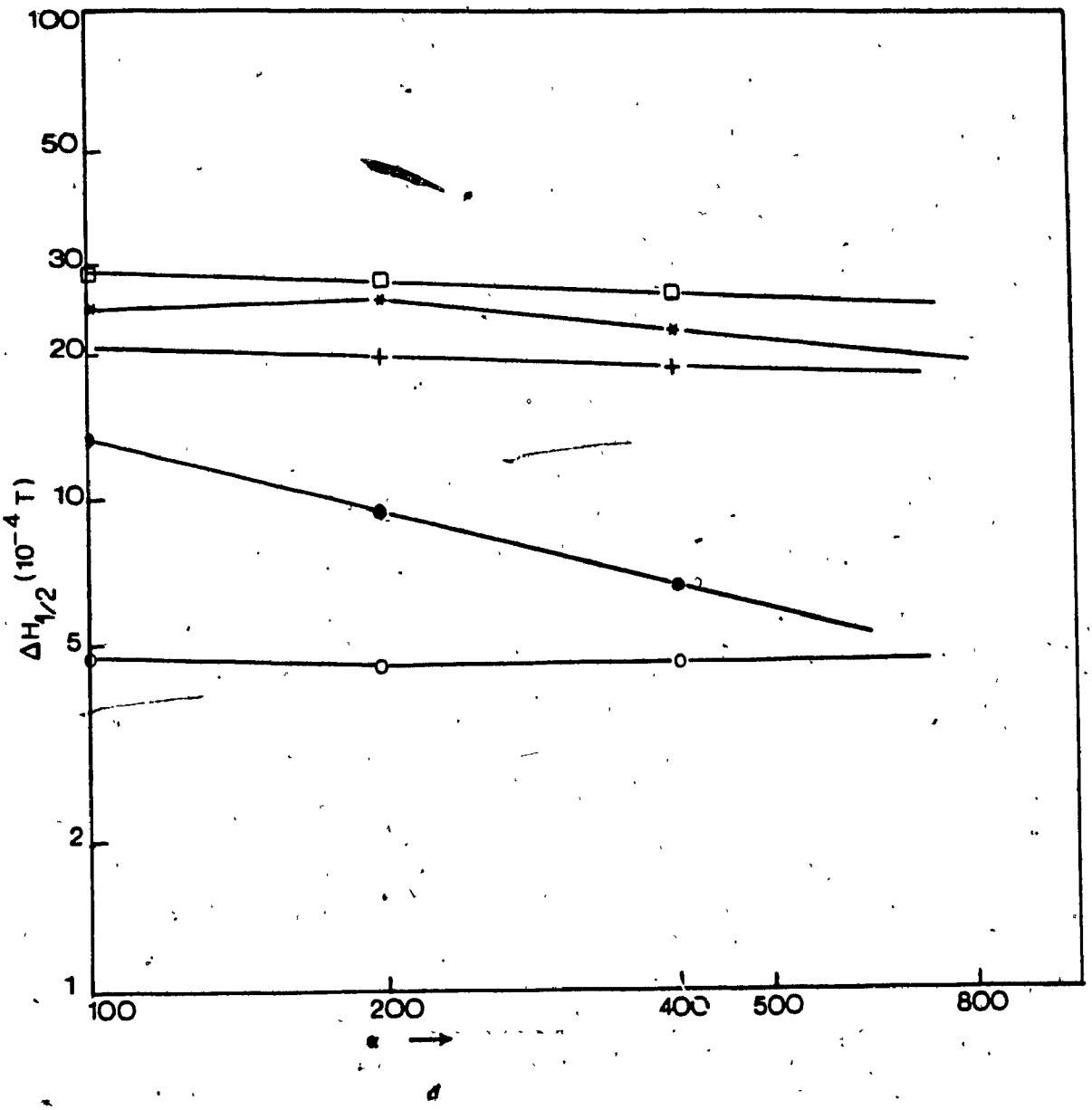


Figure 13: Log $\Delta H_{1/2}$ vs. log $\alpha$, for $\alpha \geq 100$ in $Yb_{0.5}Y_{0.5}$ CH.A:□, B:○, C:●, D:*, Sum:+.

decrease with decreasing temperature, this corresponds to a narrowing as temperature drops. This phenomenon is explained by Misra and Mikolajczak[3] in the following way "as the temperature is lowered ,the $Yb^{3+}$ spin lattice relaxation time increases and approaches the $Gd^{3+}$ spin — lattice relaxation time; then it is possible for the $Gd^{3+}$ ions to relax via the intermediary of the $Yb^{3+}$ ions, thus a narrowing of $Gd^{3+}$ lines will result". This phenomenon of narrowing of $Gd^{3+}$ linewidth as $\tau_{Yb} \rightarrow \tau_{Gd}$ (i.e. $\alpha \rightarrow 1$) is, however not observed experimentally. In fact, in experiments $Gd^{3+}$ linewidth broadens as temperature is lowered. But this is explained by the fact that even at low temperatures $\tau_{Yb} << \tau_{Gd}$ , thus $Yb^{3+}$ spin lattice relaxation time does not approach the $Gd^{3+}$ spin lattice relaxation time. However such a "fictitious" condition can be simulated theoretically and the narrowing as $\tau_{Yb} \longrightarrow \tau_{Gd}$ can be shown as $\alpha \longrightarrow 1$.

As $\alpha$ goes up from 10 to 75, there is a slight narrowing ($38 \times 10^{-4} \longrightarrow 32 \times 10^{-4}$ T) and at $\alpha$=100 the broadest linewidth ($44 \times 10^{-4}$ T) is found from the simulation. After the peak at $\alpha$=100 linewidths start getting narrower with a constant slope (fig.14). In order for random frequency narrowing to take place $\tau_{Yb}$ has to be much smaller than $\tau_{Gd}$. Since starting at $\tau_{Gd}/\tau_{Yb}$=100 and going to higher values of there is a narrowing of $Gd^{3+}$ linewidths, it can be concluded that the spin-lattice relaxation narrowing starts at $\alpha$=100.

Thus below $\alpha$=100, $\tau_{Yb}$ is not short enough to cause a narrowing. Since Anderson and Weiss'[12] and Kubo and Tomita's[8] theories of random frequency modulation narrowing is applicable, for YbCH at temperatures T≥180 K (Appendix 1) and since narrowing of linewidths is observed for $\alpha$>100, comparison of the 180-300 K temperature range will be made with the results of the simulation for $\alpha$ in the 100 to 800 range.

The ratio of linewidth at 180 K to the linewidth at 300 K observed experimentally by Misra and Sharp[4] is 1.6, this may correspond to the ratio of linewidths in the simulation at $\alpha$=120 and 800, thus

$$\Delta H_{1/2}(180\ K)/\Delta H_{1/2}(300\ K)=\Delta H_{1/2}(\alpha=120)/\Delta H_{1/2}(\alpha=800)=1.6 \quad (37)$$

The ratio of $Gd^{3+}$ linewidths at 180 K to the linewidths at 300 K observed experimentally by Malhotra et al.[2] is also 1.6. After examining the values of experimental linewidths in 180-30 K range and theoretical linewidths in the range $\alpha$=120 to 800 the following relation can be deduced:

$$\log(\alpha) \propto T \quad (38)$$

A plot of log $\Delta H_{1/2}$ vs. log $\alpha$ as well as vs. temperature is shown in fig.14 in the T=170 to 300 K and $\alpha$=100 to 800 range. From these plots it can be concluded that in the range 170-300 K (i.e.$\alpha$=100 to 800) both the experimental

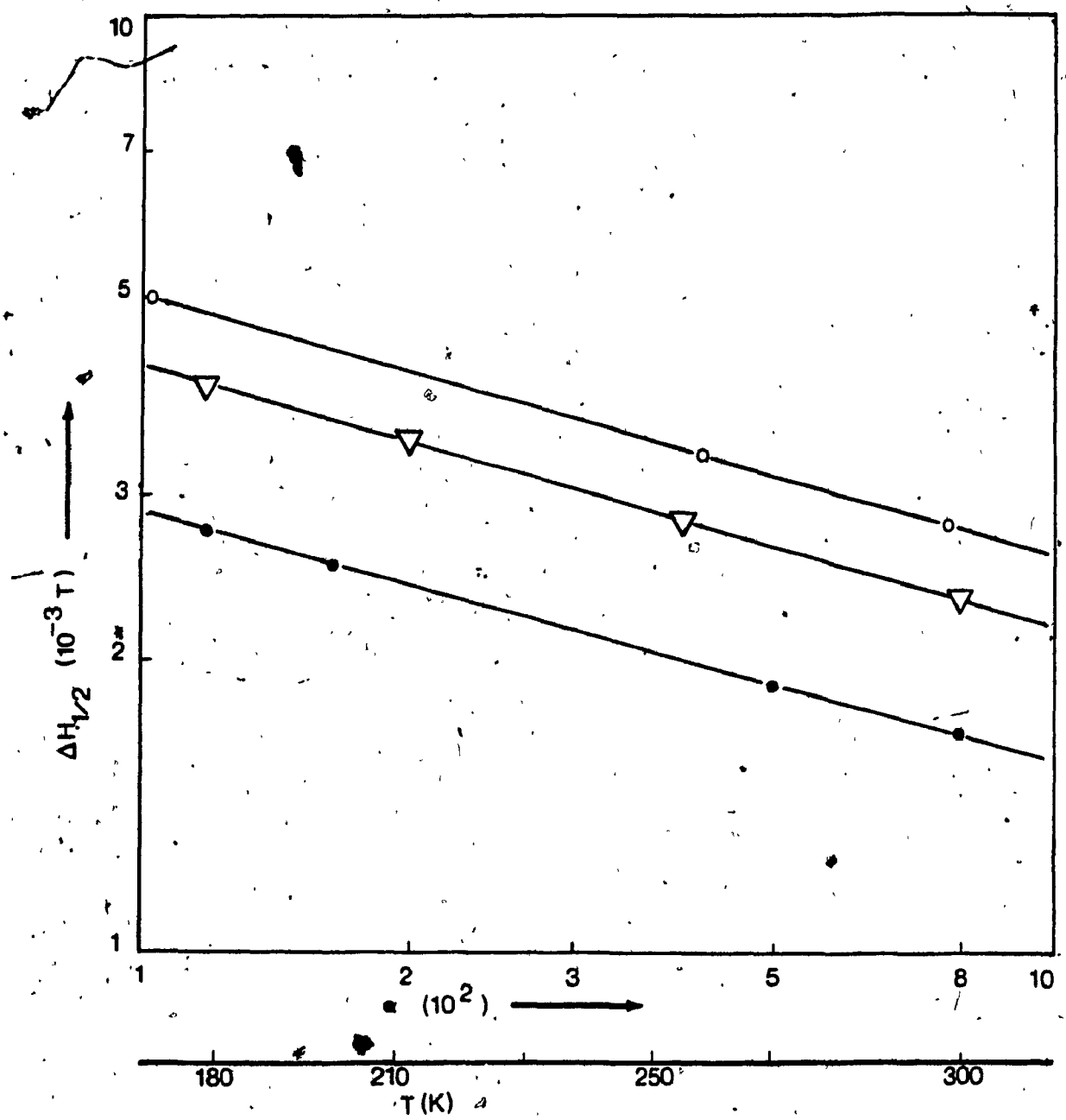


Figure 14: Log of both the experimental and simulated linewidths vs. log $\alpha$ and temperature. •:Misra and Sharp[1], o:Malhotra et al.[2], ▽:Simulated

linewidths and the theoretical linewidths narrow at the same rate. Also, the calculated linewidths are narrower than those observed by Malhotra et.al[2] and broader than those observed by Misra and Sharp[1]. Since only the spin-lattice relaxation narrowing mechanism has been considered, and since the rate of narrowing observed experimentally and simulated theoretically are in good agreement, it can be concluded that the narrowing of $Gd^{3+}$ EPR linewidths in the 180-300 K range is mainly due to the random modulation of dipolar effects by the spin-lattice relaxation process of $Yb^{3+}$ ions.

## 6.5 COMPARISON OF THEORETICAL RESULTS FOR $Yb_{0.5}Y_{0.5}CH$

Experiments done with $Yb_{0.5}Y_{0.5}CH$ crystals by Misra and Mikolajczak[3] indicate broader linewidths above 160 K than those for YbCH. However simulated linewidths give narrower linewidths for $Yb_{0.5}Y_{0.5}CH$ than for YbCH for the configurations B, C, and D. Configuration A gives broader linewidths in the range $\alpha$=1.2 to 5 and at $\alpha$>500. The sum of all four configurations also gives narrower linewidths which are approximately not varying in the range $\alpha$=10 to 400. If the same correspondence of $\alpha$ and T is made for configuration A as that in YbCH case, the rate of narrowing is found to be in good agreement with experiments (fig.15). However, in this case $\Delta H_{1/2}$ values differ by a factor of 2.

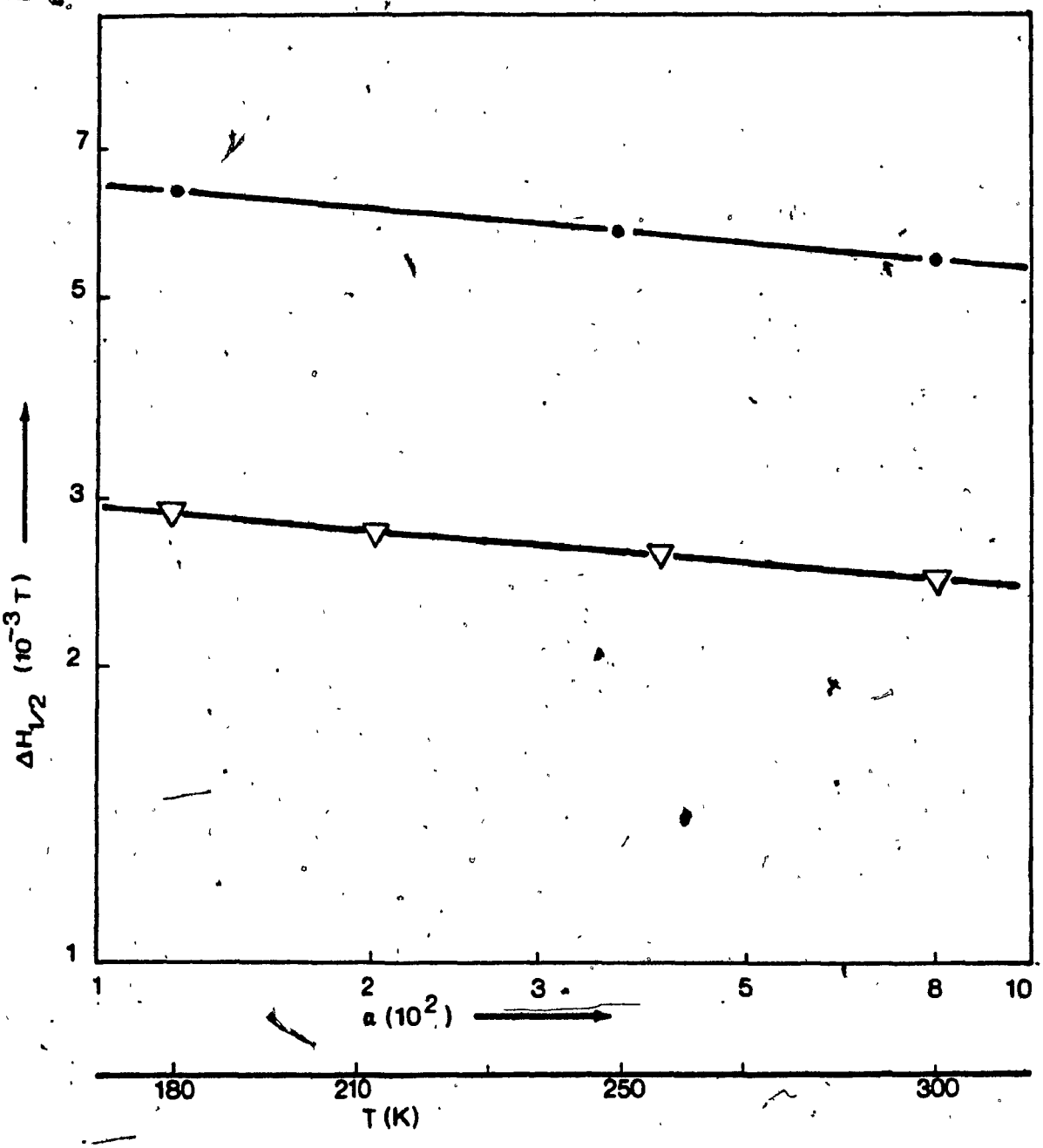


Figure 15: Log of the experimental and simulated linewidths vs. logα and temperature; ●:Experimental, ▽:Simulated.

Thus, in the case of $Yb_{0.5}Y_{0.5}CH$ crystals it can be concluded that the most likely crystal structure is the configuration A, where the unit cells alternate. The experimental and theoretical linewidths narrow by the same amount in the 180-300 K (i.e.$\alpha$=120 to 800) range, but the theoretical $\Delta H_{1/2}$ values are smaller than the experimental values (fig.15).

## 6.6 ESTIMATION OF $Gd^{3+}$ SPIN LATTICE RELAXATION TIME IN YbCH

The theoretically estimated $Yb^{3+}$ spin lattice relaxation times change by a factor of 10 in between 180 and 300 K:

$$\tau_{Yb}(180\ K)/\tau_{Yb}(300\ K)=10 \qquad (39)$$

Keeping the correspondence between and T as follows:

$$\tau_{Gd}(180\ K)/\tau_{Yb}(180\ K)=150 \qquad (40)$$

$$\tau_{Gd}(300\ K)/\tau_{Yb}(300\ K)=800 \qquad (41)$$

from (40) and (41)

$$(\tau_{Gd}(300\ K)/\tau_{Yb}(300\ K)) \times (\tau_{Yb}(180\ K)/\tau_{Gd}(180\ K))=5.66 \qquad (42)$$

and from (39)

$$(\tau_{Gd}(300\ K)/\tau_{Yb}(300\ K))x(10\ \tau_{Yb}(300\ K)/\tau_{Gd}(180\ K))=6.66 \quad (43)$$

$$\tau_{Gd}(180\ K)=1.5\,\tau_{Gd}(300\ K) \quad (44)$$

according to which $\tau_{Gd}$ is smaller at 300 K than at 180 K. Using $\alpha=120$, $\tau_{Gd}(180\ K)=8.4x10$ sec. and using $\alpha=800$, $\tau_{Gd}(300\ K)=5.6x10^{-11}$ sec. From this data following temperature dependence can be shown:

$$\tau_{Gd} \propto T^{-0.8} \quad (45)$$

Using $\tau_{Gd}(300\ K)$ and $\tau_{Gd}(180\ K)$ this can be written as

$$\tau_{Gd}=5.35x10^{-9}\,T^{-0.8} \quad (46)$$

in YbCH crystals in the 180-300 K range.

# CHAPTER 7

## CONCLUSION

In Chapter 2, the theory of $Yb^{3+}$ spin-lattice relaxation time was studied. An expression to calculate $\tau_{Yb}$ in YbCH, without using the observed linewidths was derived (eq.(7)). This equation gives $\tau_{Yb}$ values which agree with Anderson's equation (eq.(2)) and therefore enables the calculation of theoretical $\Delta H_{1/2}$ values. In order to confirm the narrowing of EPR linewidths due to random frequency modulation, so that eq.(7) can be used in Anderson's equation (eq.(2)), a computer simulation using a Monte Carlo method was adapted. The results, discussed in Chapter 6 are in good agreement with the experimental values in the 180-300 K range where Anderson's equation (eq.(2)) is applicable to YbCH. In the case of the $Yb_{0.5}Y_{0.5}CH$ crystal, calculated linewidths were smaller than the experimental ones by a factor of two, but none the less showed narrowing with increasing $\alpha$ value, by the same amount as observed in experiments in the 180-300 K range. This indicates that the narrowing is mainly due to the spin-lattice relaxation process of $Yb^{3+}$ ions and Anderson's equation can be used to estimate the $Yb^{3+}$ spin-lattice relaxation times in $Yb_{0.5}Y_{0.5}CH$.

## REFERENCES


1. S.K.Misra and G.R.Sharp, J.Phys.C10, 897(1977)
2. V.M.Malhotra, H.A.Buckmaster, and J.M.Dixon, J.Phys.C13,3921(1980)
3. S.K.Misra and P.Mikolajczak, Phys.stat.sol.(b), 109,59(1982)
4. J.Soeteman, L.Bevaart, and A.J.Van Duyneveldt, Physica(Utrecht), 74, 126(1974)
5. G.M.Kalvius, G.K.Shenoy, and B.D.Dunlap, Proc.XVI.Congr.Ampere, Bucharest 1970(p.584)
6. M.Fierz, Physica V,no 5, 433(1938)
7. P.W.Anderson, J.Phys.Soc.Japan.9, 316(1954)
8. R.Kubo and K.Tomita, J.Phys.Soc.Japan.9, 888(1954)
9. A.Abragam and B.Bleaney, Electron Paramagnetic Resonance of Transition Ions(Clarendon, Oxford, 1970)
10. J.H.Van Vleck, Phys.Re.74, 1168(1948)
11. G.J.Gorter and J.H.Van Vleck, Phys.Rev.72, 1128(1947)
12. P.W.Anderson and P.R.Weiss, Rev.Mod.Phys, 25, 269(1953)
13. T.Mitsuma, J.Phys.Soc.Japan, 17, 128(1962)
14. G.E.Pake and T.L.Estle, The Physical Principles of Electron Paramagnetic Resonance, (W.A.Benjamin, Reading, Massachusetts 1973)
15. S.K.Misra and G.R.Sharp, J.Phys.Chem.Solids, 37, 999(1976)

## APPENDIX 1

## CONDITIONS FOR THE APPLICABILITY OF EXCHANGE NARROWING THEORY TO MODULATION NARROWING

Mitsuma[13] discussed the following conditions so that if they are fullfilled , the exchange theories of Anderson and Weiss[12] could be applied to the spin lattice relaxation (modulation) narrowing: (i) $[H_{mod}, H\ ]=0$; (ii) $[H_{mod}, S^{Gd}\ ]=0$; (iii) $H_{mod} >> H_{dip}$ ; (iv) $H_{dip}$ must be so small as to have no important matrix elements connecting different unperturbed states of $H_z$. Here $H_{mod}$ is the Hamiltonian responsible for the modulation of the dipolar fields on the $Gd^{3+}$ ions due to superposition of the spin orbit coupling and the orbit lattice coupling in $Yb^{3+}$ ions, where the magnitude of $H_{mod}$ in field scale is given by eq.(14). $H_z = g\,\mu_B\, H_o \sum_j S_{z_j}^{Gd}$ (in field scale =0.3 Tesla) and $H_{dip}$ represents the dipolar interaction of the $Gd^{3+}$ ion with the $Yb^{3+}$ ions, given in field scale by eq.(13).

Conditions (i) and (ii) are fulfilled, as $H_{mod}$ contains the spin operators of the $Yb^{3+}$ ion while $H_z$ contains the spin operators of $Gd^{3+}$ ion ; thus the two commutators in (i) and (ii) are between different spins. Condition (iv) is satisfied, since $H_z$ is determined by a field on the avarage of $3000 \times 10^{-4}$ T and $H_{dip} << H_{mod}$. Condition (iii) is satisfied only at higher temperatures ($T \geq 180$ K) where spin

lattice relaxation time of the $Yb^{3+}$ ions presumably becomes quite small .

## APPENDIX 2

### DERIVATION OF EQUATION (25)

In order to derive equation (25), Bloch's equations have to be used. These can be written as:

$$d\bar{M}/dt=\gamma\bar{H} \times \bar{M} \tag{47}$$

$$dM_x/dt=\gamma(H_y M_z-H_z M_y) \tag{48}$$

$$dM_y/dt=\gamma(H_x M_z-H_z M_x) \tag{49}$$

$$dM_z/dt=\gamma(H_x M_y-H_y M_x) \tag{50}$$

where $H_{x'}$ is along x'-axis and it corresponds to $H_1$ in Chapter 4. $H_{y'}=0$, since there is no field along y'-axis. $H_z$ is the total field along z,z' axis and can be written as:

$$H_z=(\upsilon_L+\upsilon_N)/\gamma \tag{51}$$

Using eq.(51) and letting x',y',z' rotate with a frequency $\nu_N$ Bloch's equations can be rewritten as:

$$dM_{x'}/dt=-(\upsilon_L+\upsilon_N)M_{y'} \tag{52}$$

$$dM_{y'}/dt=-\upsilon_N M_{z'}+(\upsilon_L+\upsilon_N)M_{x'} \tag{53}$$

$$dM_z/dt = \nu_N M_y' \tag{54}$$

Equation (22) from chapter 4:

$$M_T = M_y' \sin\Phi + M_x' \cos\Phi \tag{22}$$

can be differentiated yielding:

$$dM_T/dt = \dot{M}_y' \sin\Phi + \dot{M}_x' \cos\Phi + M_y' \cos\Phi \, d\Phi/dt - M_x' \sin\Phi \, d\Phi/dt \tag{55}$$

Since a phase angle $\Phi$ can be written as:

$$\Phi = \sum_i \nu_i \Delta t_i \tag{56}$$

$d\Phi/dt$ can be written as:

$$d\Phi/dt = \nu_N + \nu_L \tag{57}$$

Substituting eqs. (52),(53), and (57) into (55) yields:

$$dM_T/dt = -\nu_N M_z' \sin\Phi \tag{25}$$

which when integrated yields:

$$M_{T_2} = M_{T_1} - \frac{\nu_N M_z'}{\nu_N + \nu_L} (\cos\Phi_1 - \cos\Phi_2) \tag{26}$$

## APPENDIX 3

### LISTING AND THE FLOWCHART OF THE PROGRAM

```
00100 PROGRAM GAU3(INPUT,OUTPUT,TAPE5)
00110 DIMENSION WL(10),CN(10),NS(10)
00120 REAL R(15000)
00130 INTEGER NR
00140 DOUBLE PRECISION DSEED
00150 NR=15000
00160 I2=0
00170 DSEED=1*123457.D0
00180C LOAD GAUSSIAN DISTRIBUTED
00190C RANDOM NUMBERS
00200 CALL GGNML(DSEED,NR,R)
00210 HY=0.0
00220C ENTER GD AND YB RELAXATION TIMES
00230 TAU=1E-5
00240 TAU1=25.00E-5
00270 WL(1)=-4.4069E8
00280 WL(2)=WL(1)
00290 WL(3)=4.0595E7
00300 WL(4)=WL(3)
00310 WL(5)=WL(3)
00320 WL(6)=WL(5)
```

```
00330 WL(7)=-5.6379E7
00340 WL(8)=WL(7)
00350 WL(9)=WL(8)
00360 WL(10)=WL(9)
00370C CALCULATE G LARMOR FREQUENCY DUE
00380C TO EXTERNAL FIELD
00390 OML=(1.988*9.27E-24*.3)/6.626E-34
00400 DO 77 J=1,1000
00410C SET YB IONS UP OR DOWN RANDOMLY
00420 DO 78 K=1,10
00430 SR=RANF()
00440 IR=NINT(SR)
00450 IF (IR .EQ.  1) GO TO 78
00460 WL(K)=-WL(K)
00470 78 CONTINUE
00480 HP1=0.0
00490 PH2=0.0
00500 D=0.
00510 SIGMA=1.0
00520 DT=TAU/100
00530 RANGE=.5*TAU
00540 CONVER1=RANGE/(3.*SIGMA)
00550 PHI=0.0
00560 OMEG1=WL(1)+WL(2)+WL(3)+WL(4)+
00570+WL(5)+WL(6)+WL(7)+WL(8)+WL(9)+WL(10)
00580 I=1
00590 12 CONTINUE
```

```
00600 Z=1
00610 DO 10 NG=I2,I2+9
00620 CN(Z)=CONVER1*R(NG)*SIGMA
00630 CN(Z)=TAU+CN(Z)
00640 Z=Z+1
00650 I2=I2+1
00660 IF (I2 .GE.  15000) GO TO 5
00670 GO TO 10
00680 5 DSEED=DSEED*1.25
00690 CALL GGNML(DSEED,NR,R)
00700 I2=1
00710 10 CONTINUE
00720 C=CN(1)
00730 DO 20 NK=2,10
00740 IF (CN(NK) .GT.  CN(NK-1)) C=CN(NK)
00750 20 CONTINUE
00760 D=D+C
00770 HP=0.0
00780 PHO=0.0
00790 PHI=0.0
00800C CHECK IF GD ION DECAYED
00810 IF (D .GT.  TAU1) GO TO 125
00820 I=I+1
00830C
00840 N=C/DT
00850 DO 30 L=1,N
00860 DT1=DT*EXP(-DT*(L-1)/TAU1)
```

```
00870 PHI=PHI+(OML+OMEG1)*DT1
00880 HP=HP-(OMEG1/(OML+OMEG1))*HZ*(COS(PHO)-COS(PHI))
00890 PHO=PHI
00900C CHECK IF ANY YB ION FLIPPED
00910 DO80 NO=1,10
00920 IF (L*DT .GE.  CN(NO)) GOTO 8
00930 GO TO 80
00940 8 IF (NS(NO) .EQ.  NO) GO TO 80
00950 NS(NO)=NO
00960 WL(NO)=-WL(NO)
00970 80 CONTINUE
00980 OMEG1=WL(1)+WL(2)+WL(3)+WL(4)+
009901+WL(5)+WL(6)+WL(7)+WL(8)+WL(9)+WL(10)
01000 30 CONTINUE
01010 HP1=HP1+HP
01020 PH2=PH2+PHI
01030 C=0.0
01080 GO TO 12
01090C
01110 125 CONTINUE
01120 PH2=PH2/I
01130 HP1=HP1/I
01140 PH4=AMOD(PH2,6.283)
01150 HY=HP1*SIN(PH4)
01160 PRINT*,HY
01170 A=A+1
01180 I1=I1+I
```

```
01190 77 CONTINUE
01200 STOP
01210 END
```


Start
Load Gaussian Random Numbers
Initialize Variables
Set Yb3+, Gd3+ ion relaxation times
Enter Gd 3+ Larmor freq due to Yb3+ neighbors
Calculate Gd3+ Larmor freq.due to ext. field
1

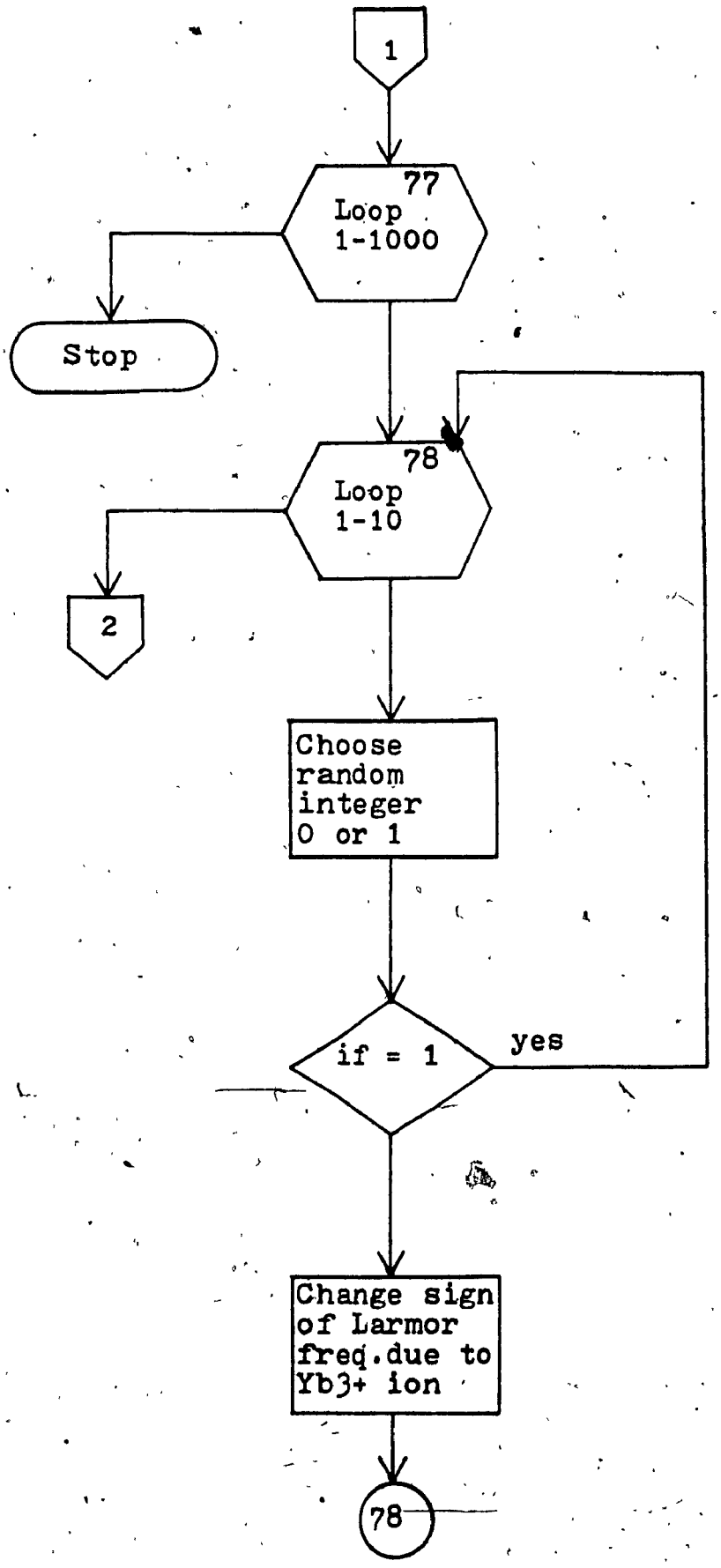
1
77
Loop
1-1000
Stop
78
Loop
1-10
2
Choose
random
integer
0 or 1
if = 1
yes
Change sign
of Larmor
freq.due to
Yb3+ ion
78

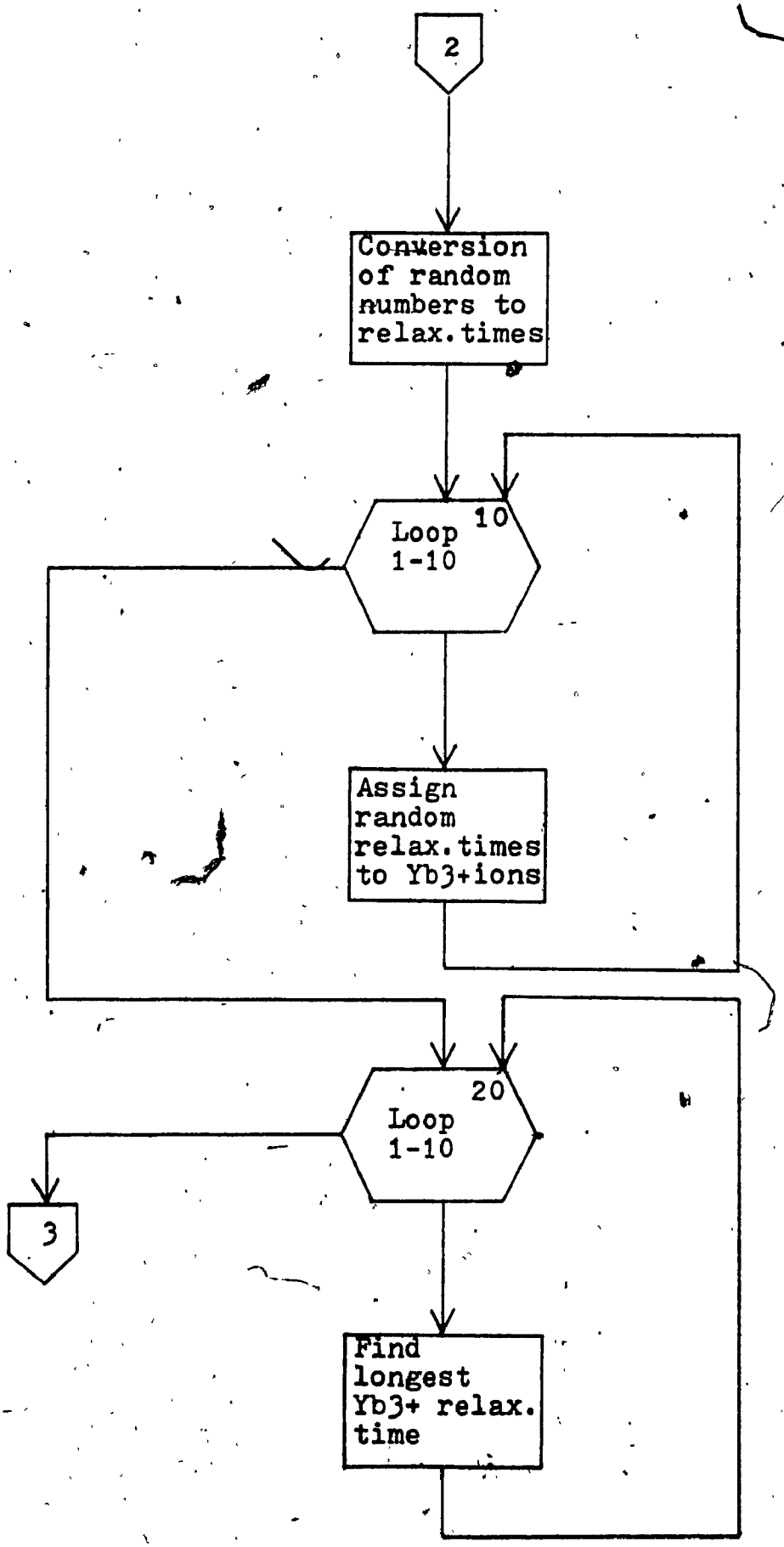
2
Conversion of random numbers to relax.times
Loop 1-10
10
Assign random relax.times to Yb3+ions
Loop 1-10
20
3
Find longest Yb3+ relax. time

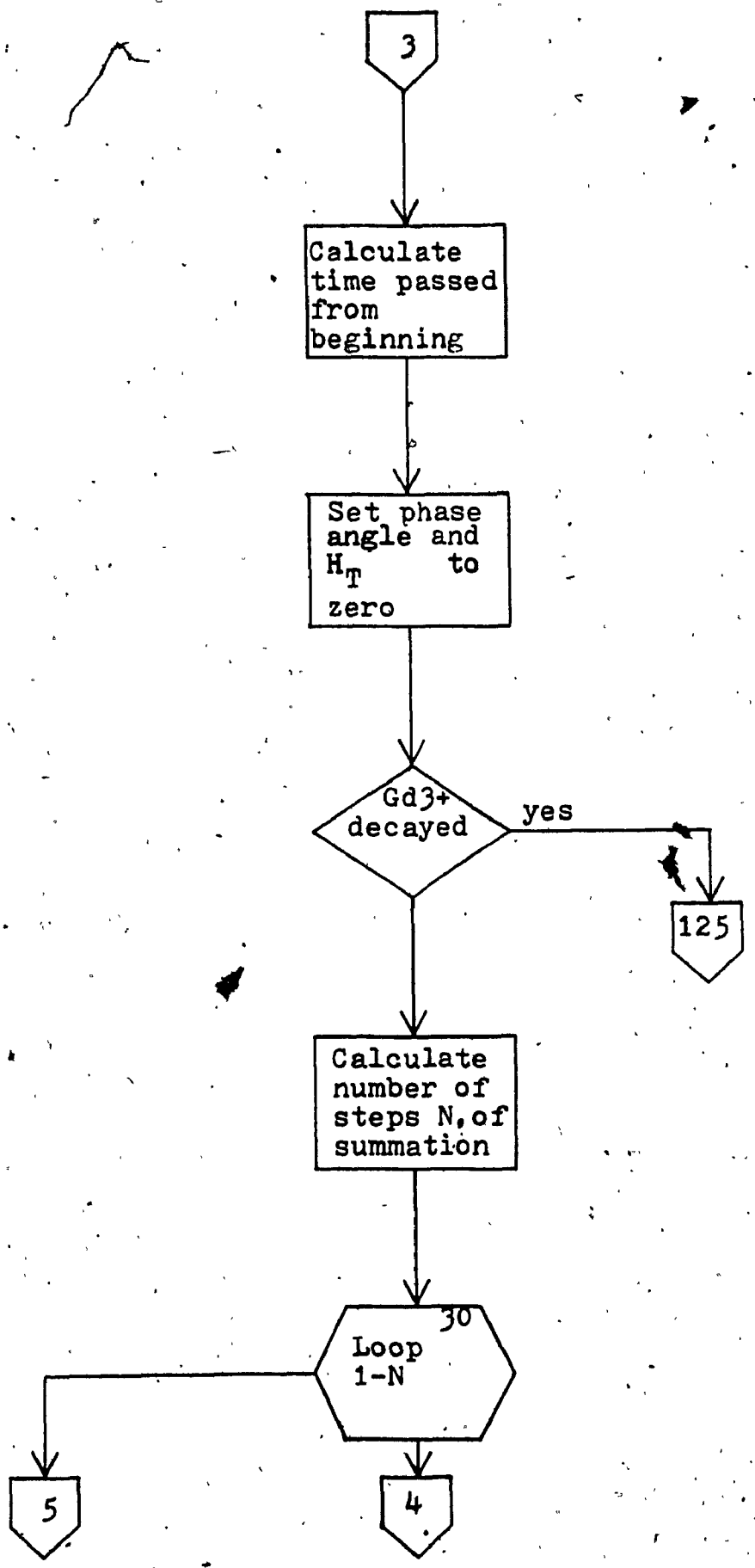
3
Calculate time passed from beginning
Set phase angle and $H_T$ to zero
Gd3+ decayed
yes
125
Calculate number of steps N, of summation
30
Loop 1-N
5
4

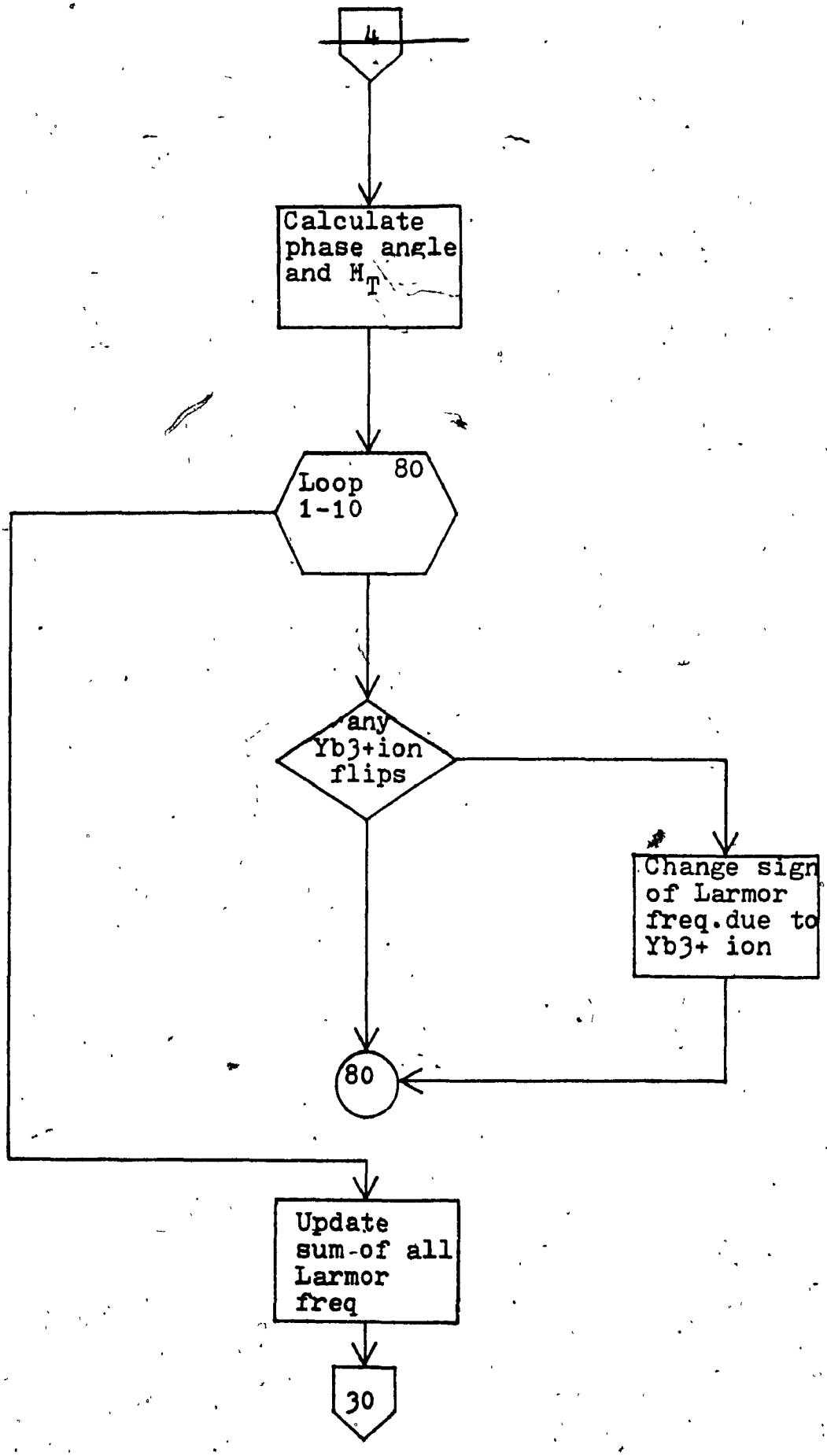
4
Calculate phase angle and $M_T$
Loop 80 1-10
any Yb3+ion flips
Change sign of Larmor freq.due to Yb3+ ion
80
Update sum-of all Larmor freq
30

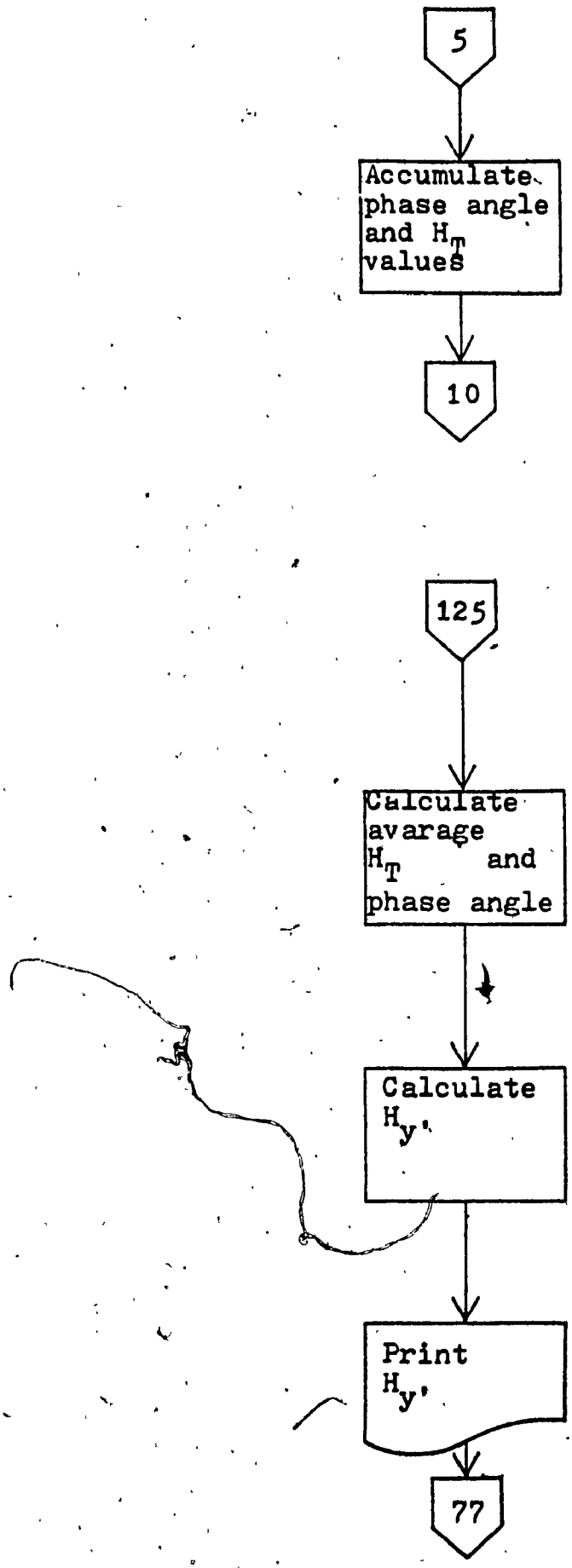
5
Accumulate phase angle and $H_T$ values
10
125
Calculate avarage $H_T$ and phase angle
Calculate $H_{y'}$
Print $H_{y'}$
77